Early Metal Di(pyridyl) Pyrrolide Complexes with Second Coordination Sphere Arene-Pi Interactions: Substrate Binding and Ethylene Polymerization

Jessica Sampson†[1], Gyeongshin Choi†, Muhammed Naseem Akhtar‡, E.A. Jaseer‡, Rajesh Theravalappil‡, Nestor Garcia‡, and Theodor Agapie†*

†Division of Chemistry and Chemical Engineering, California Institute of Technology, 1200 E California Blvd, Pasadena, CA 91125, United States.

‡Center for Refining and Petrochemicals, King Fahd University of Petroleum and Minerals, Dhahran, 31261, Saudi Arabia.

Supporting Information

[1] Current address: *Department of Chemistry, Princeton University, Princeton, New Jersey 08544, United States*

Contents

Spectra

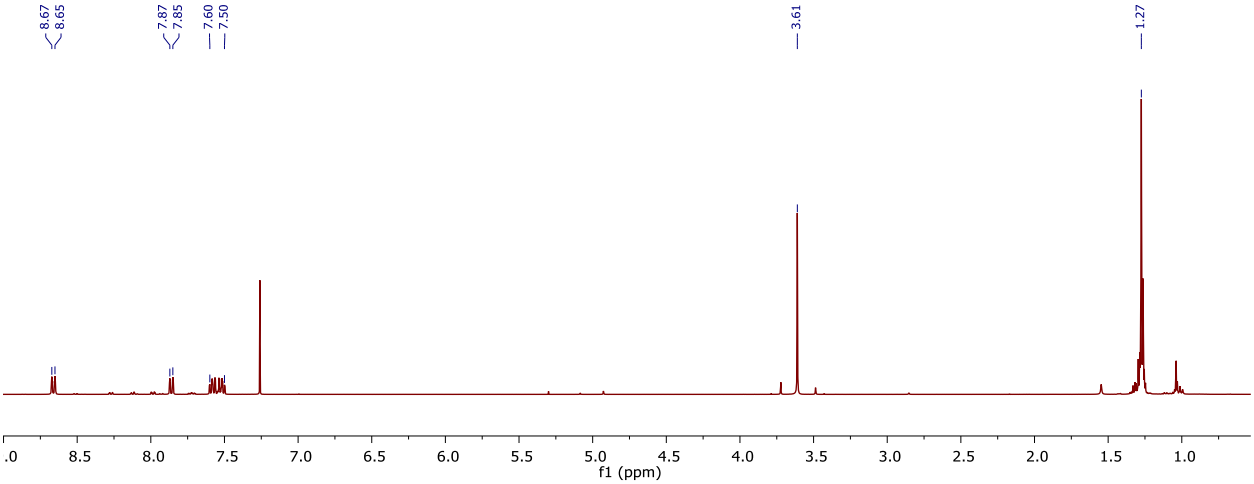

Figure S1. ^{1}H NMR spectrum of **3** in $CDCl_3$.

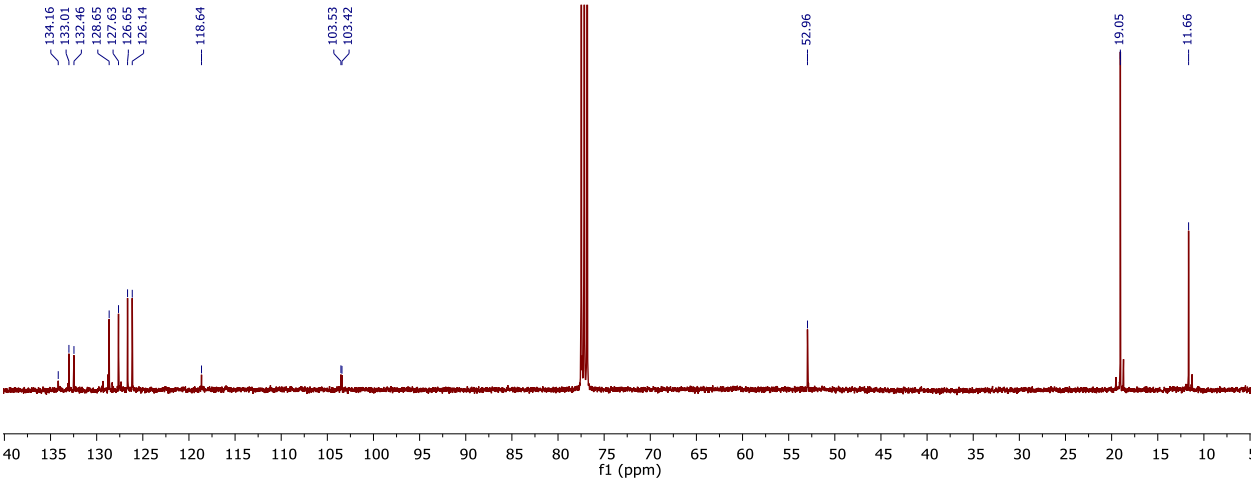

Figure S2. ^{13}C NMR spectrum of **3** in $CDCl_3$.

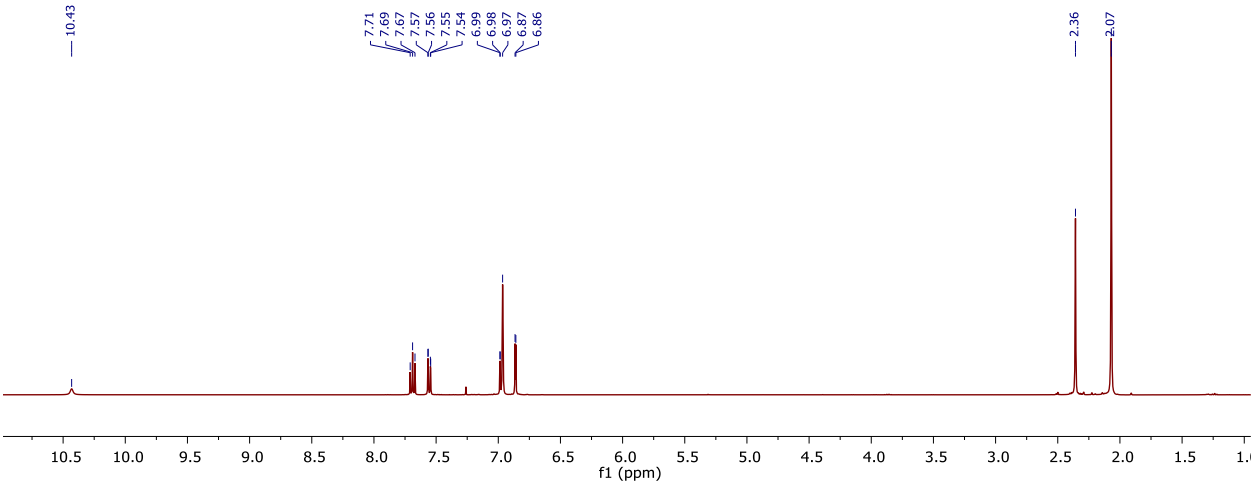

Figure S3. ^{1}H NMR spectrum of **4** in $CDCl_3$.

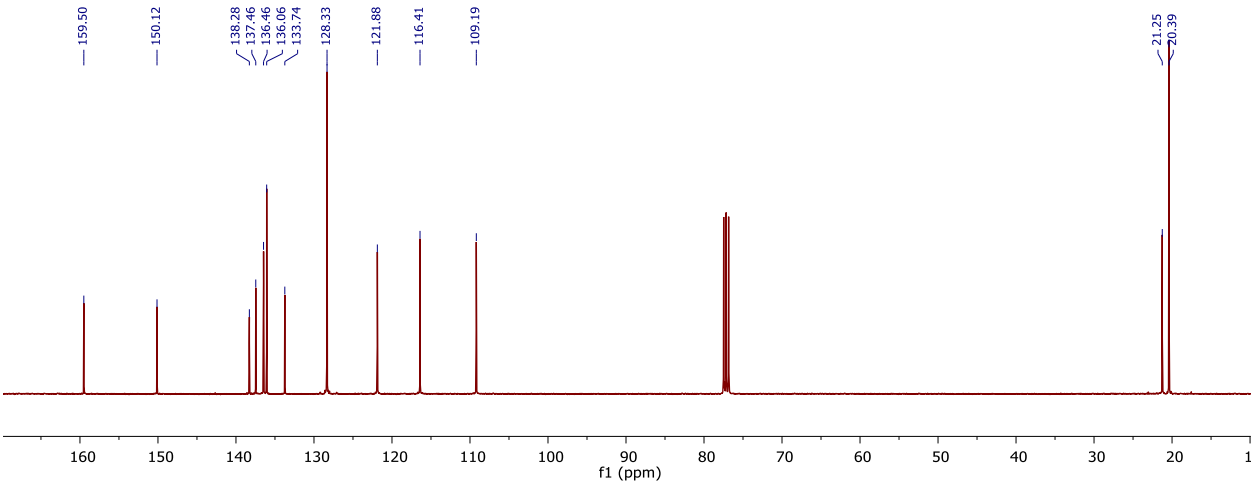

Figure S4. ^{13}C NMR spectrum of **4** in $CDCl_3$.

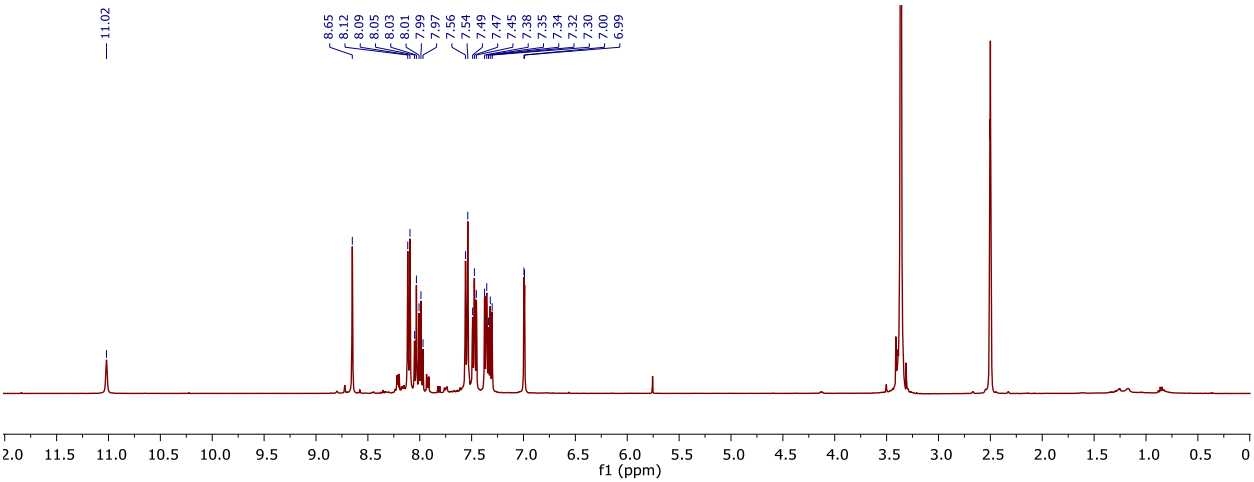

Figure S5. ^{1}H NMR spectrum of **5** in $(CD_3)_2SO$.

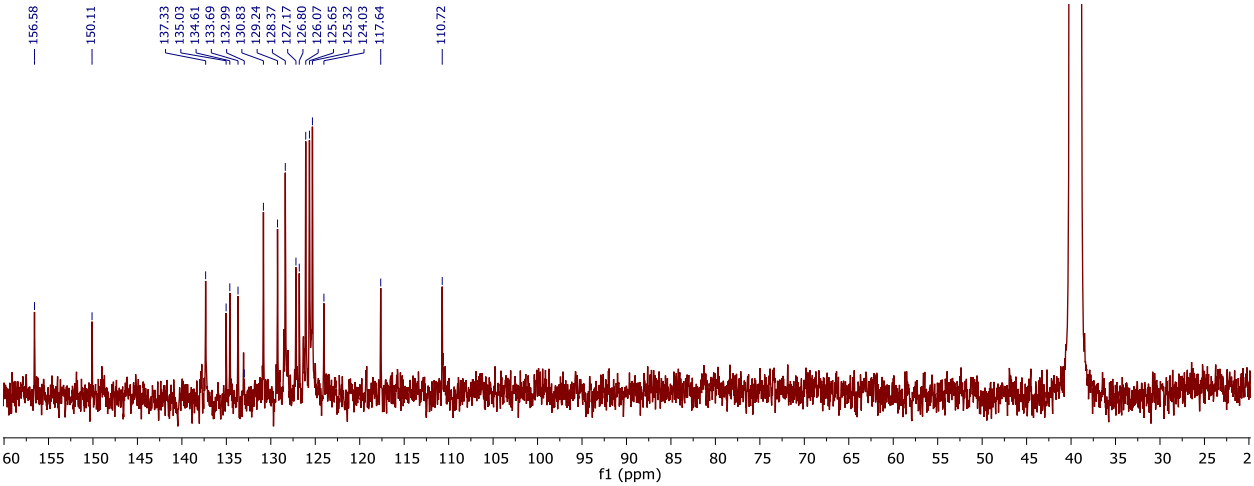

Figure S6. ^{13}C NMR spectrum of **5** in $(CD_3)_2SO$.

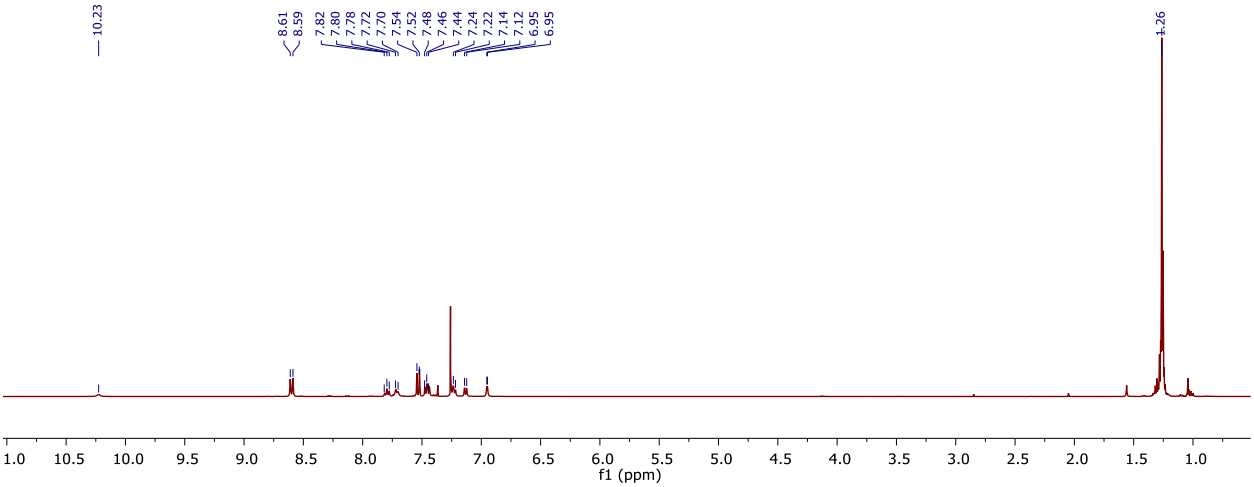

Figure S7. ^{1}H NMR spectrum of **6** in $CDCl_3$.

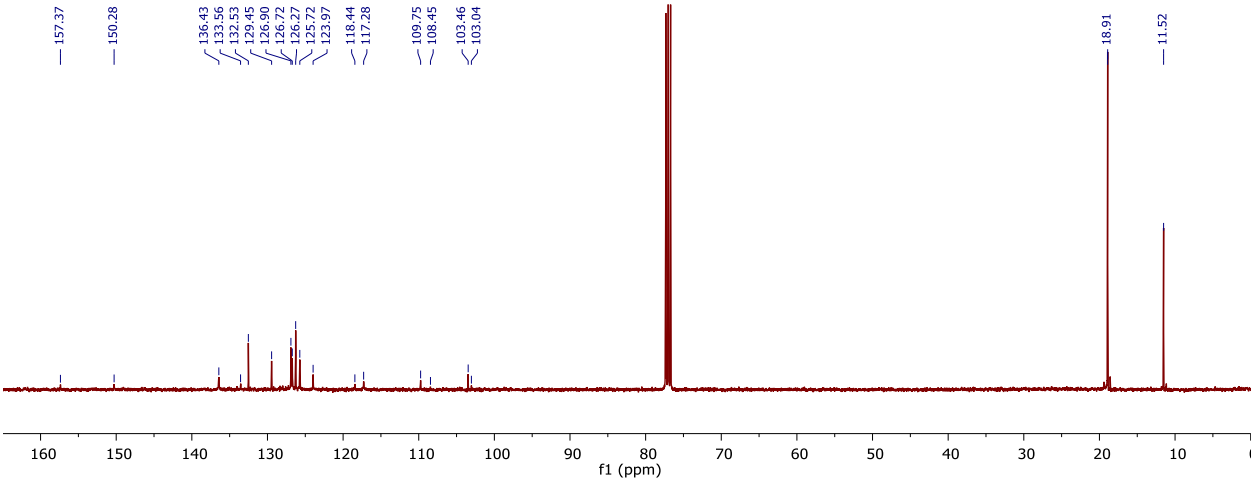

Figure S8. ^{13}C NMR spectrum of **6** in $CDCl_3$.

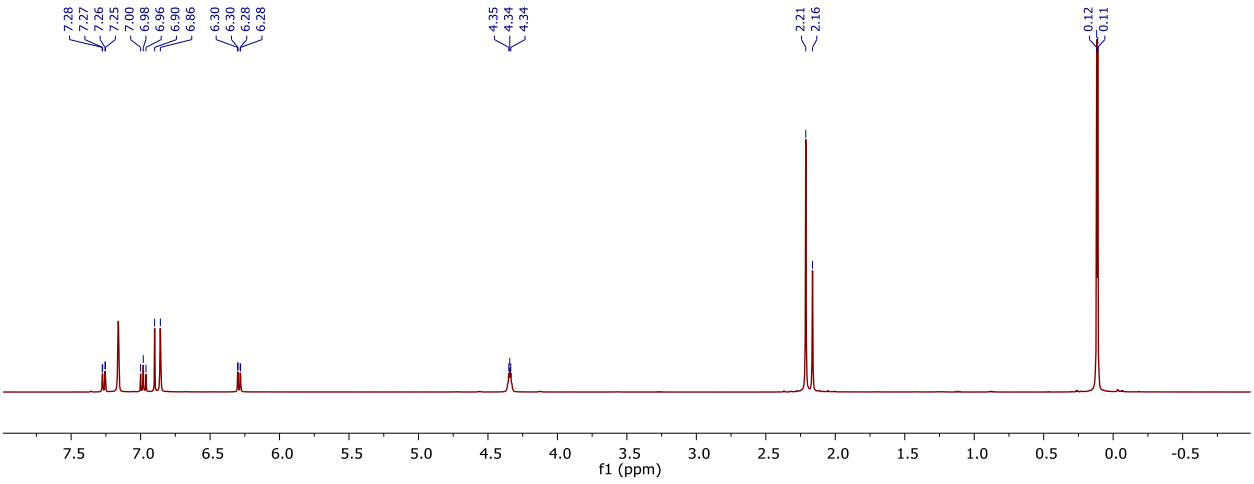

Figure S9. ^{1}H NMR of **7** in C_6D_6.

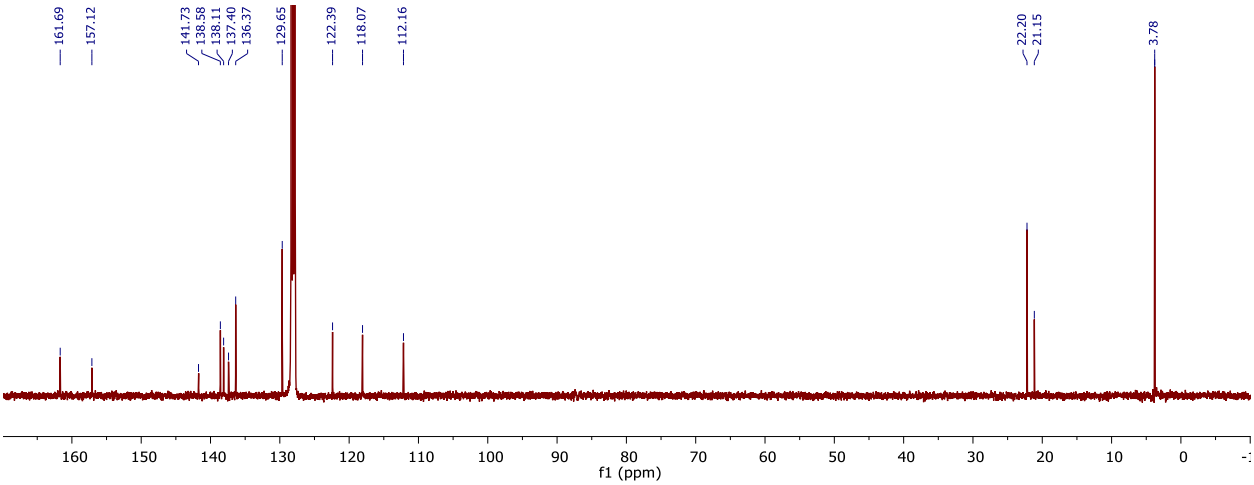

Figure S10. ^{13}C NMR of **7** in C_6D_6.

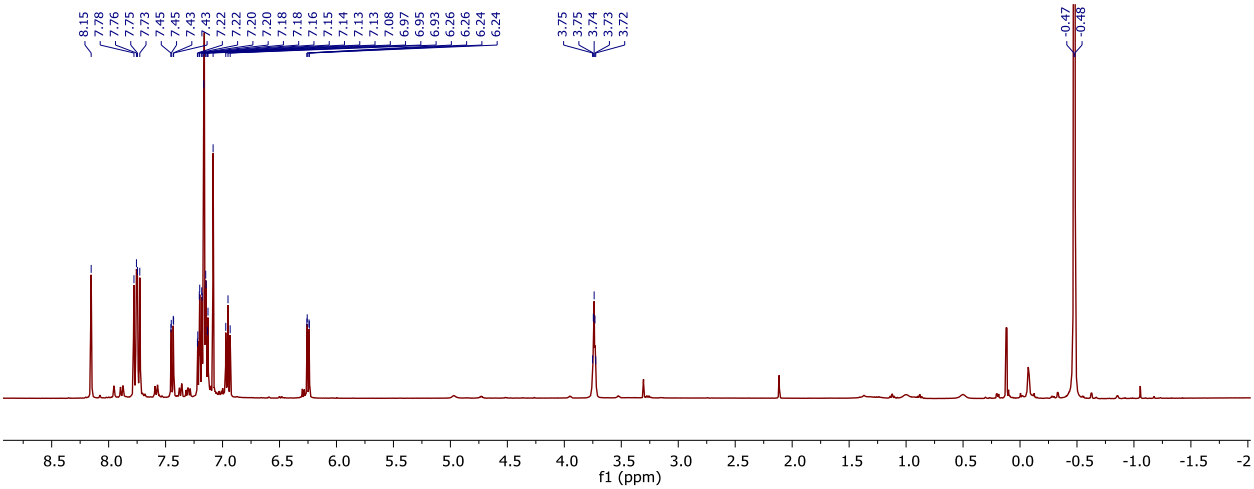

Figure S11. ^{1}H NMR of **8** in C_6D_6.

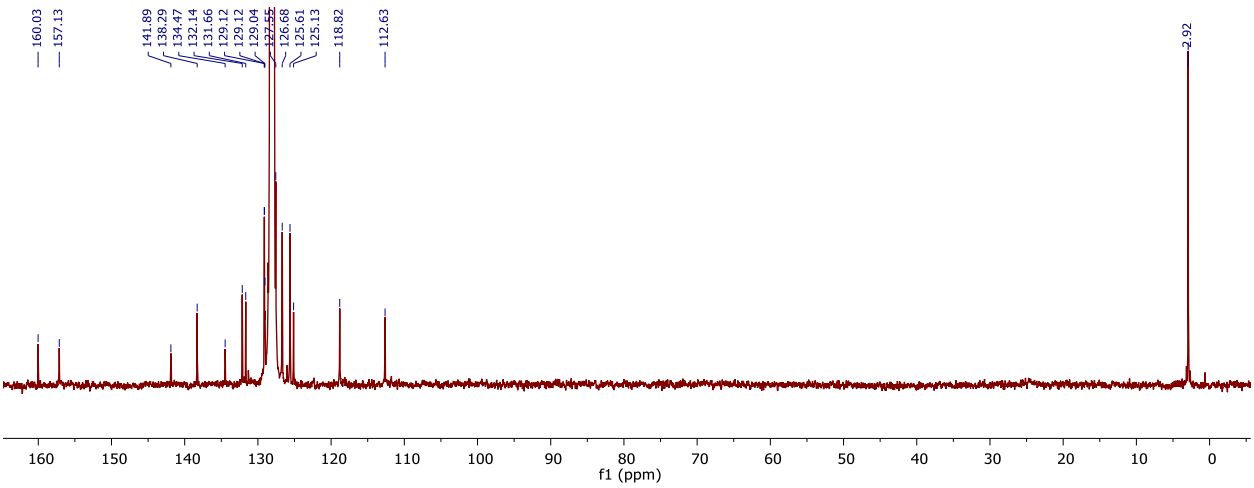

Figure S12. ^{13}C NMR of **8** in C_6D_6.

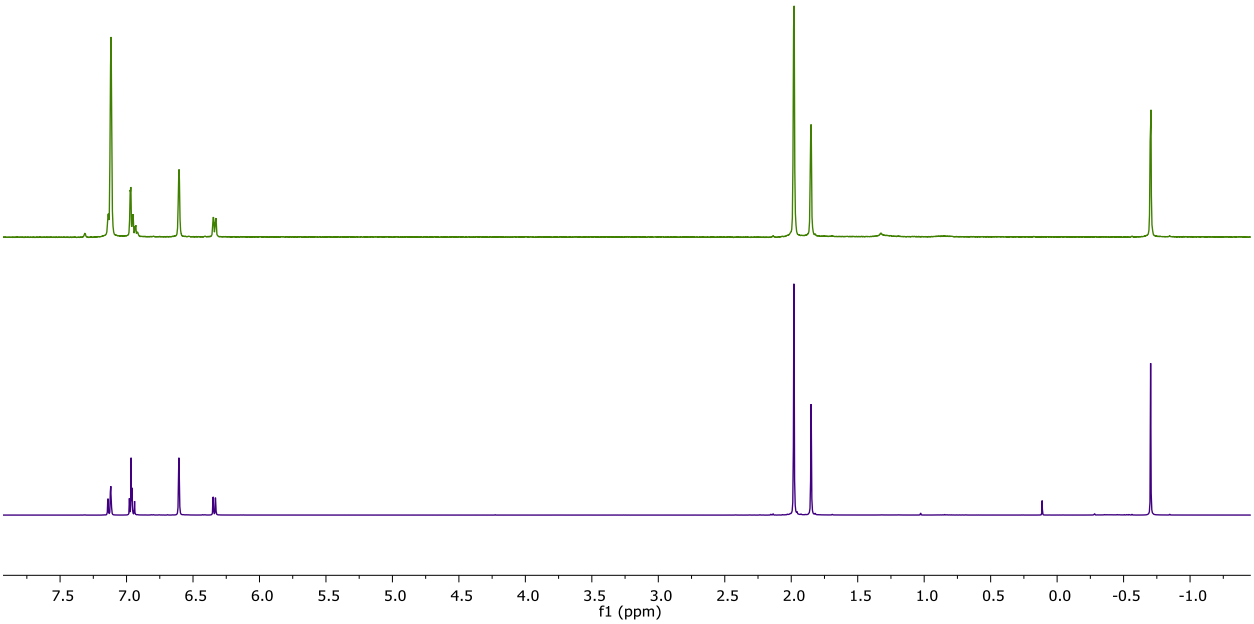

Figure S13. Comparison of the product of the reaction of **7** with $AlMe_3$ (top, green) and the product of the reaction of $(DPP^{mes})H$ (**4**) with $AlMe_3$ (**10**, bottom, blue), C_6D_6.

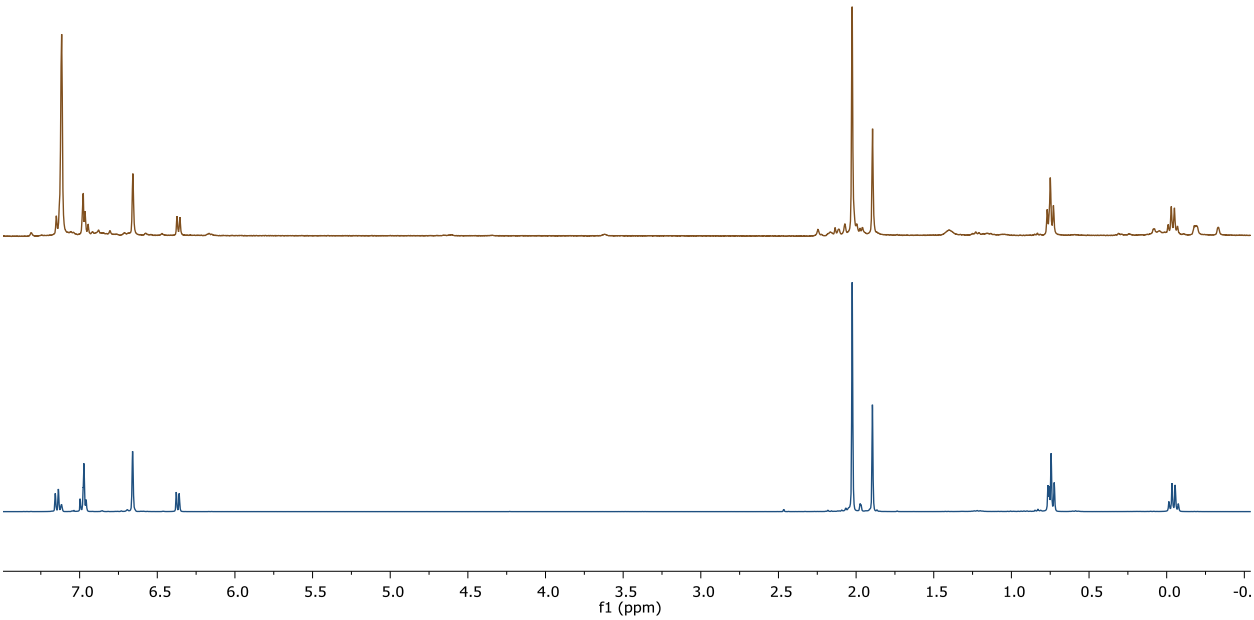

Figure S14. Comparison of the product of the reaction of **7** with $AlEt_3$ and the product of the reaction of $(DPP^{mes})H$ (**4**) with $AlEt_3$ (**11**), C_6D_6.

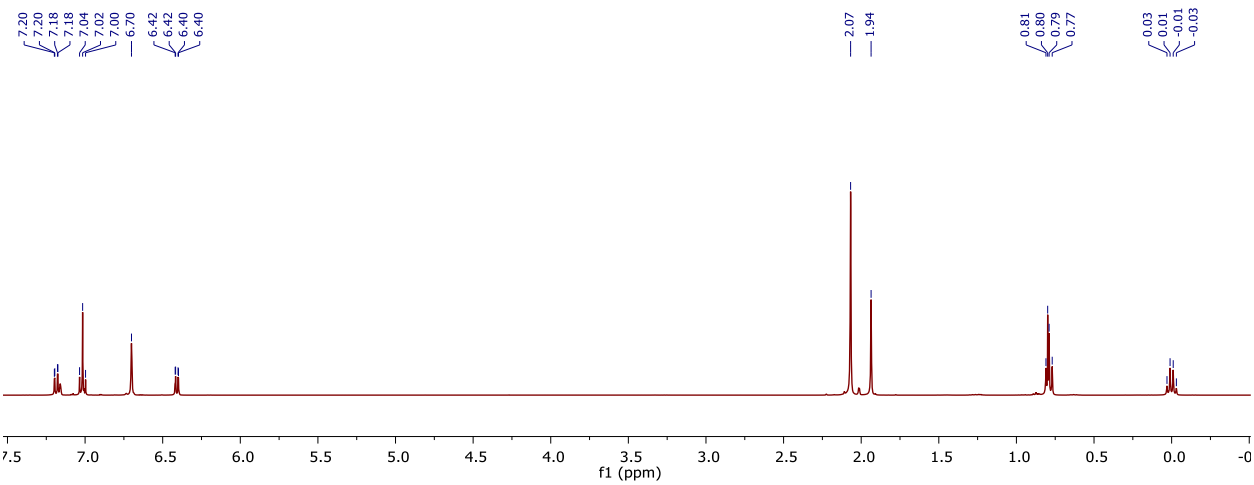

Figure S15. ^{1}H NMR of **11** in C_6D_6. The resonance at 0.80 ppm is assigned to residual ethane.

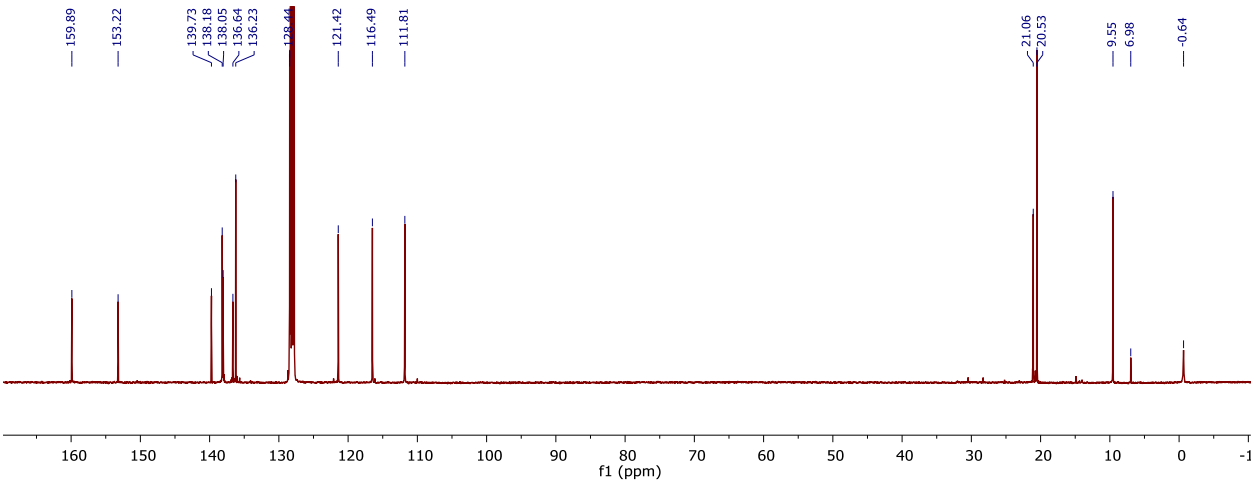

Figure S16. ^{13}C NMR of **11** in C_6D_6. The resonance at 6.98 ppm assigned to residual ethane.

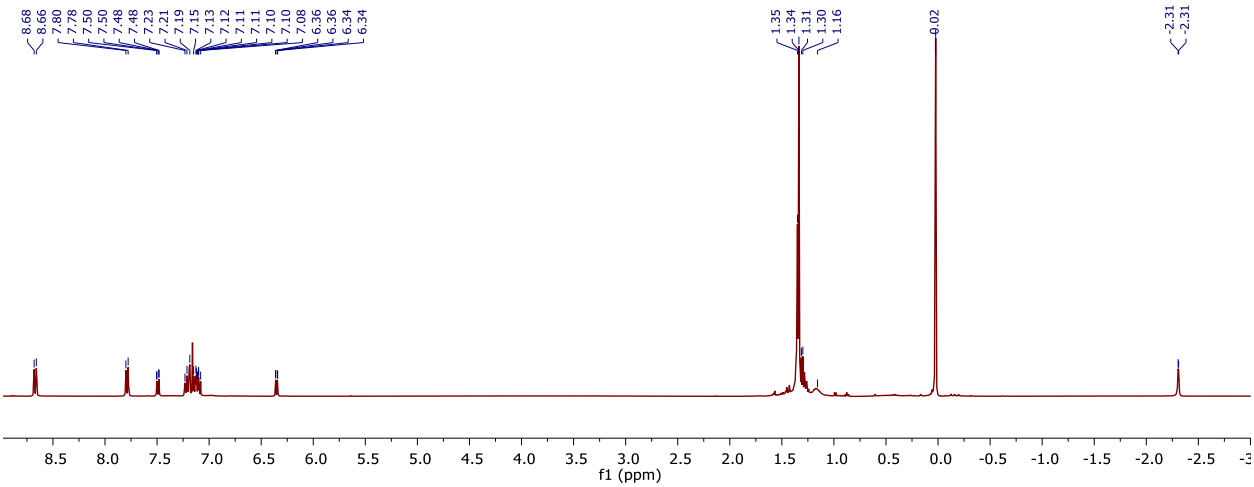

Figure S17. ^{1}H NMR of **12** in C_6D_6.

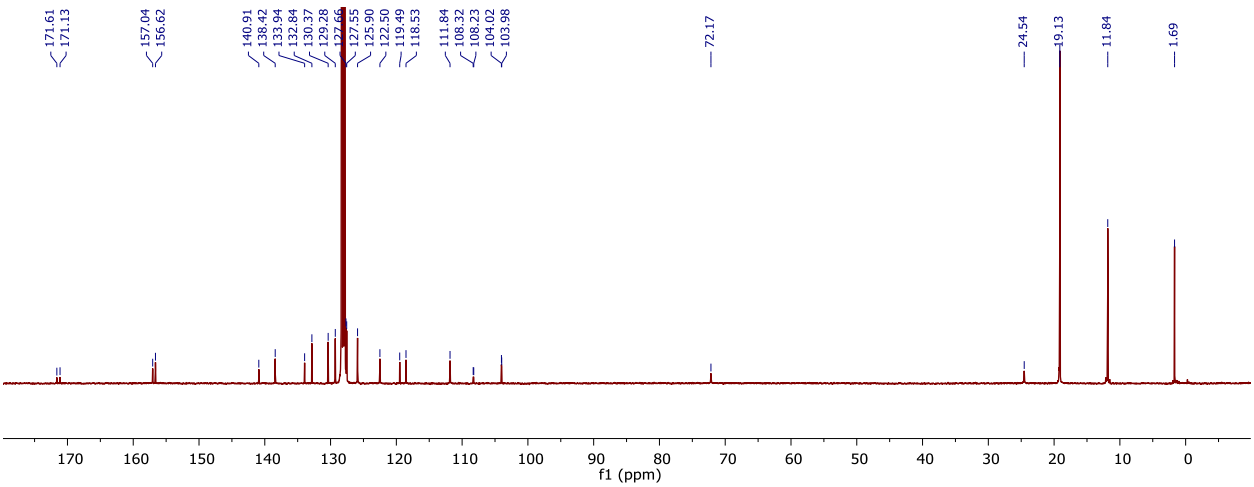

Figure S18. ^{13}C NMR of **12** in C_6D_6.

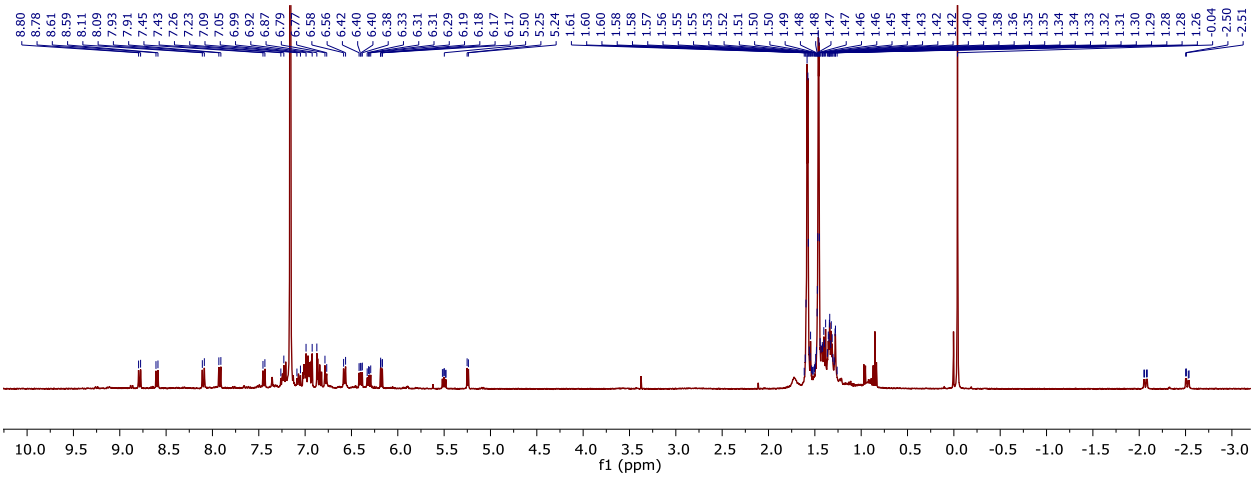

Figure S19. ^{1}H NMR of the first decomposition product of **12** in C_6D_6.

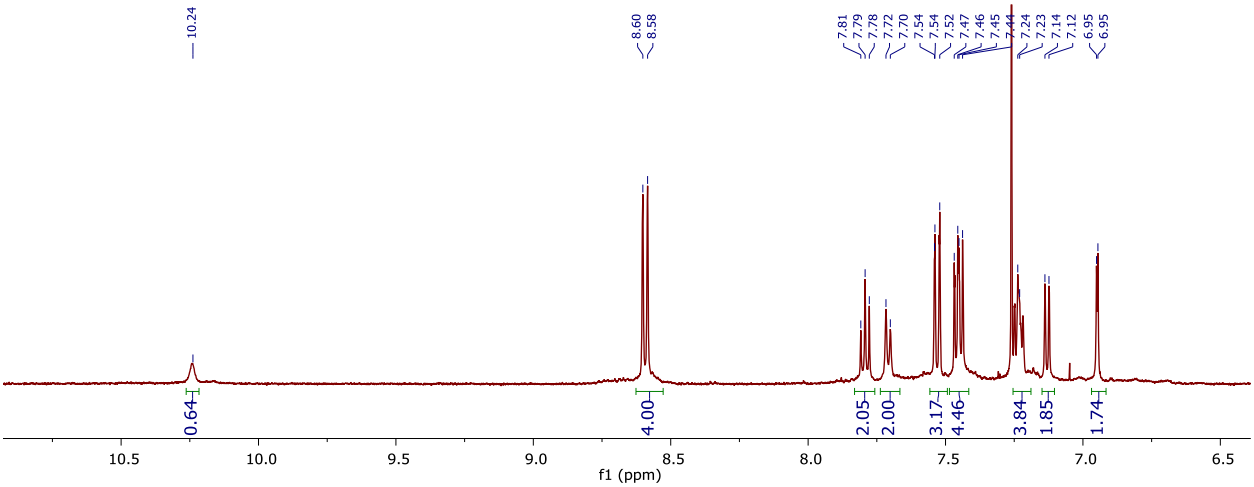

Figure S20. ^{1}H NMR of the aromatic region of the CD_3OD-quenched first decomposition product of **12** in $CDCl_3/CD_3OD$.

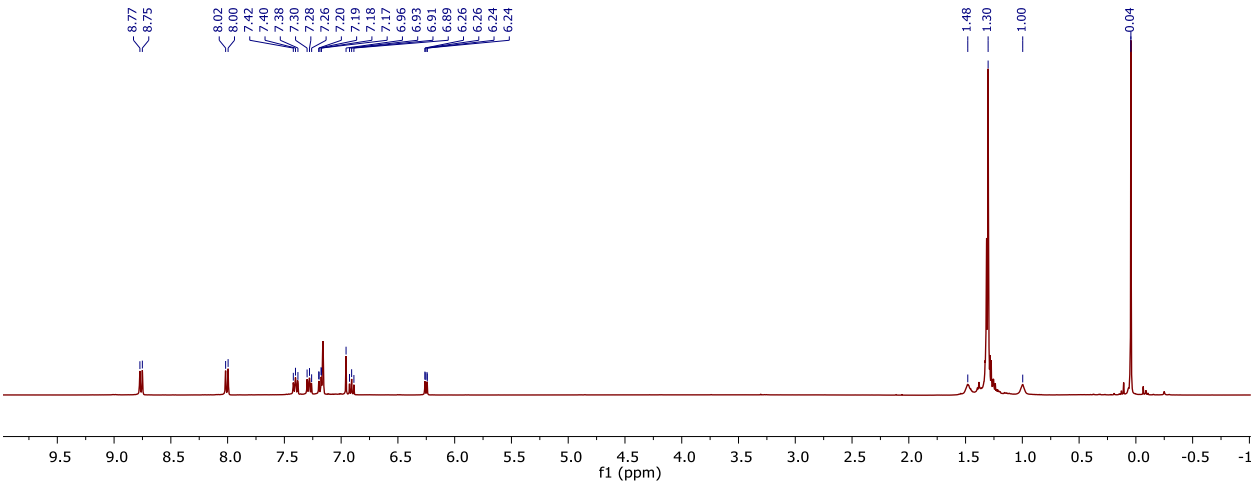

Figure S21. ^{1}H NMR of **13** in C_6D_6.

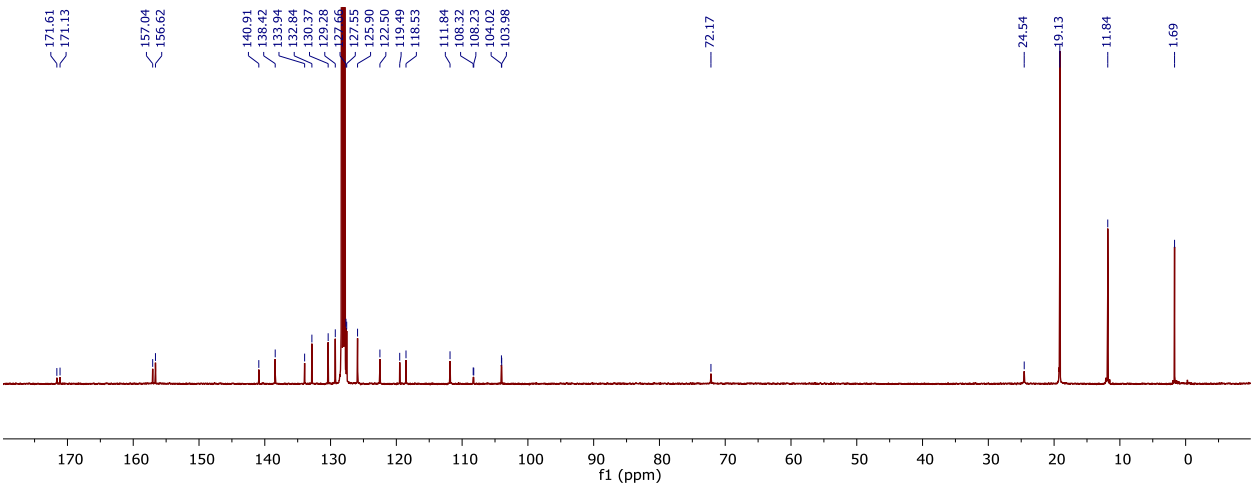

Figure S22. ^{13}C NMR of **13** in C_6D_6.

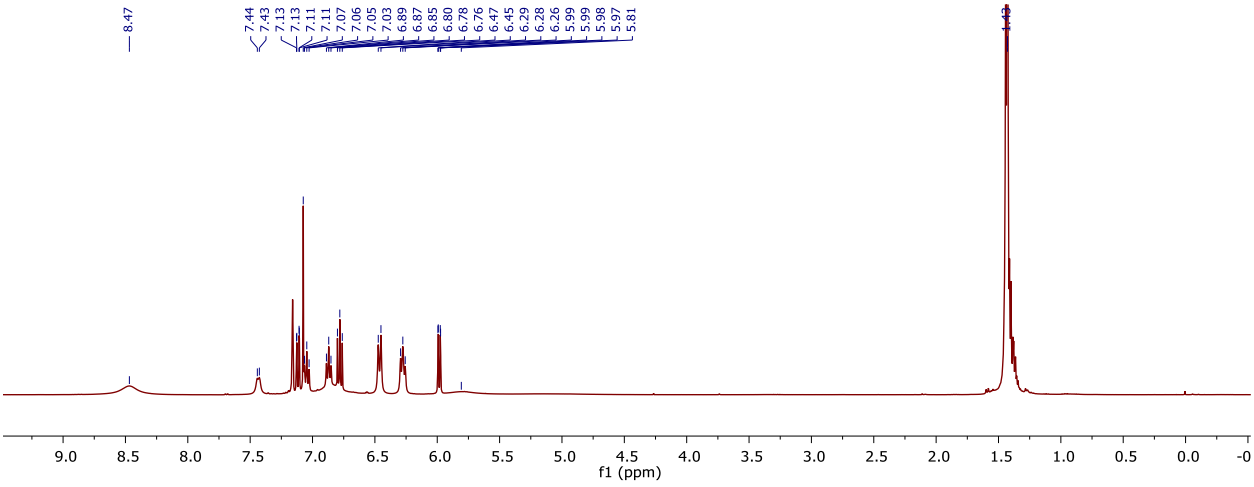

Figure S23. ^{1}H NMR of **14** in C_6D_6.

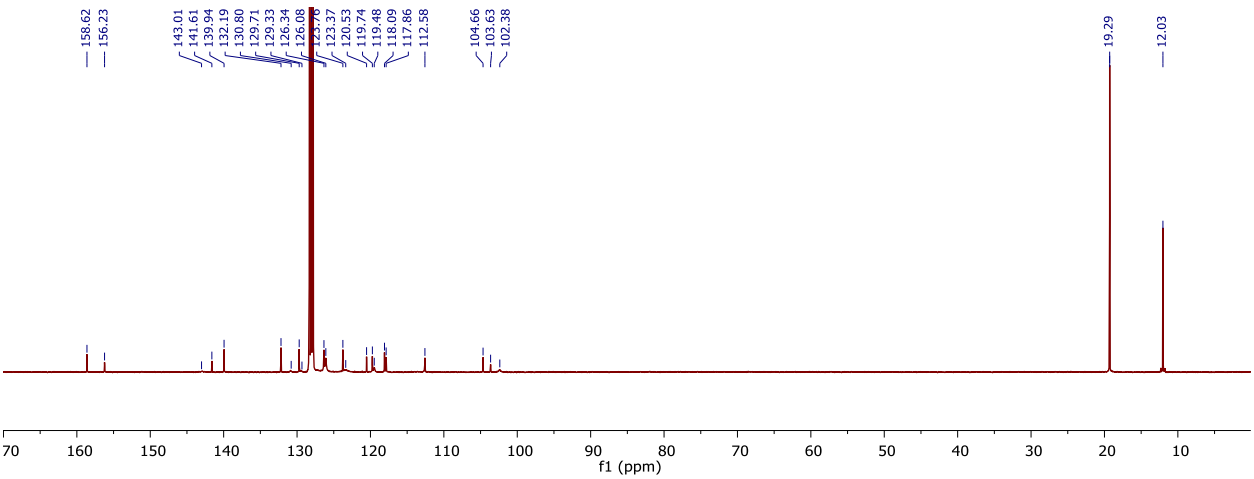

Figure S24. ^{13}C NMR of **14** in C_6D_6.

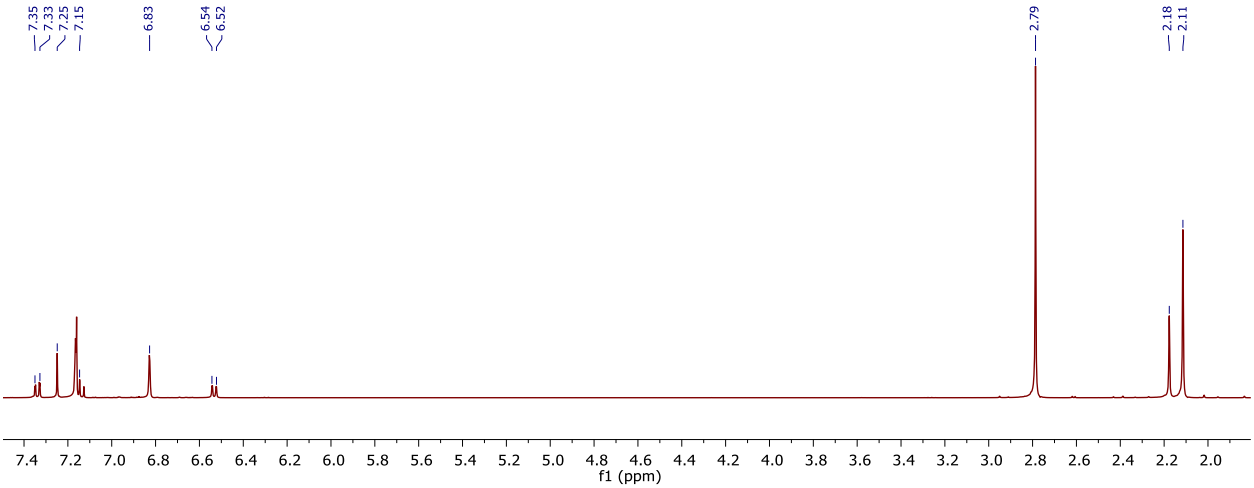

Figure S25. ^{1}H NMR spectrum of **16** in C_6D_6.

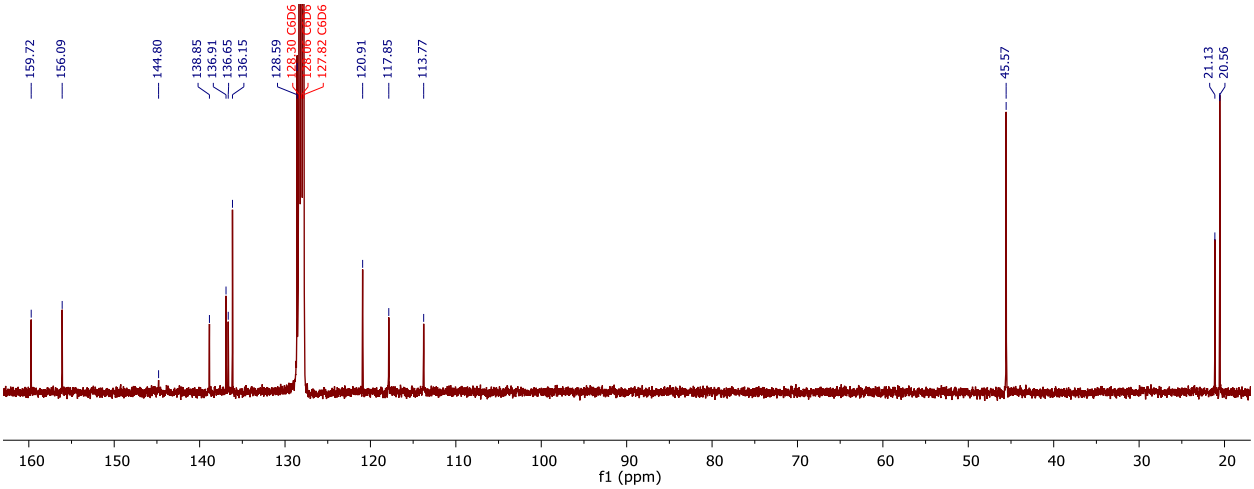

Figure S26. ^{13} NMR spectrum of **16** in C_6D_6.

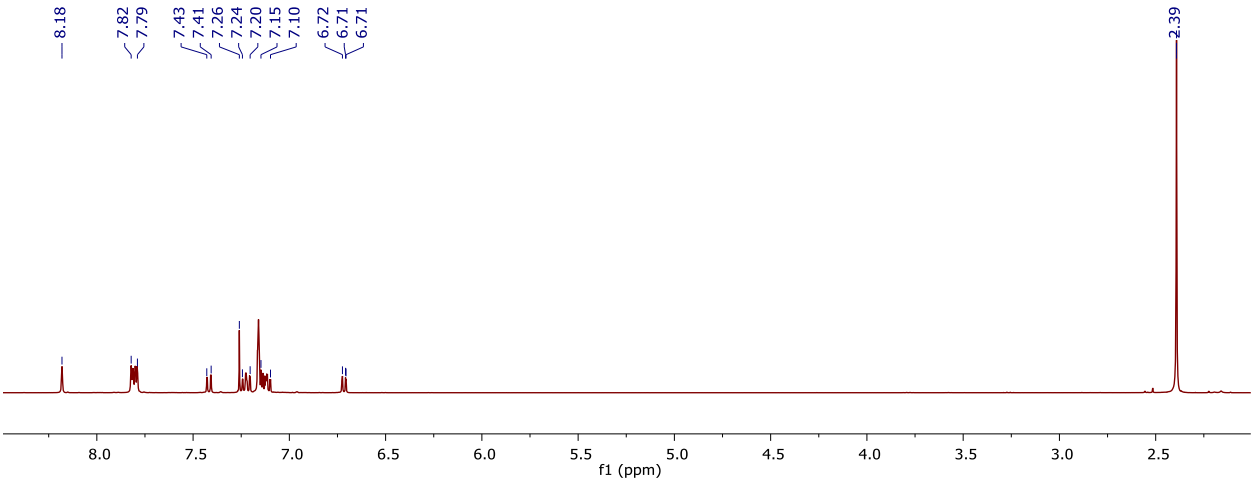

Figure S27. ^{1}H NMR spectrum of **17** in C_6D_6.

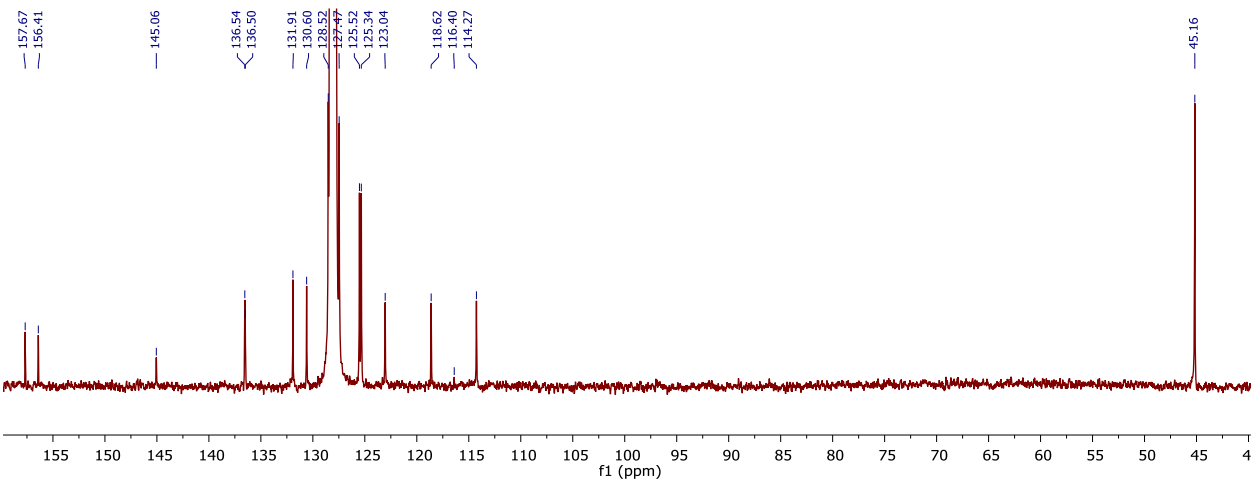

Figure S28. ^{13}C NMR spectrum of **17** in C_6D_6.

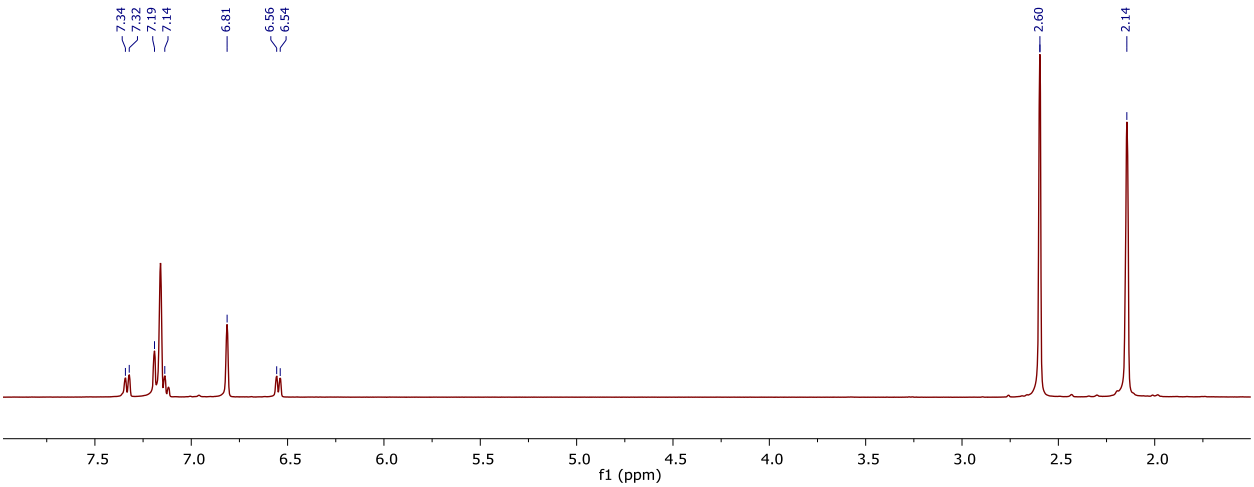

Figure S29. ^{1}H NMR spectrum of **18** in C_6D_6.

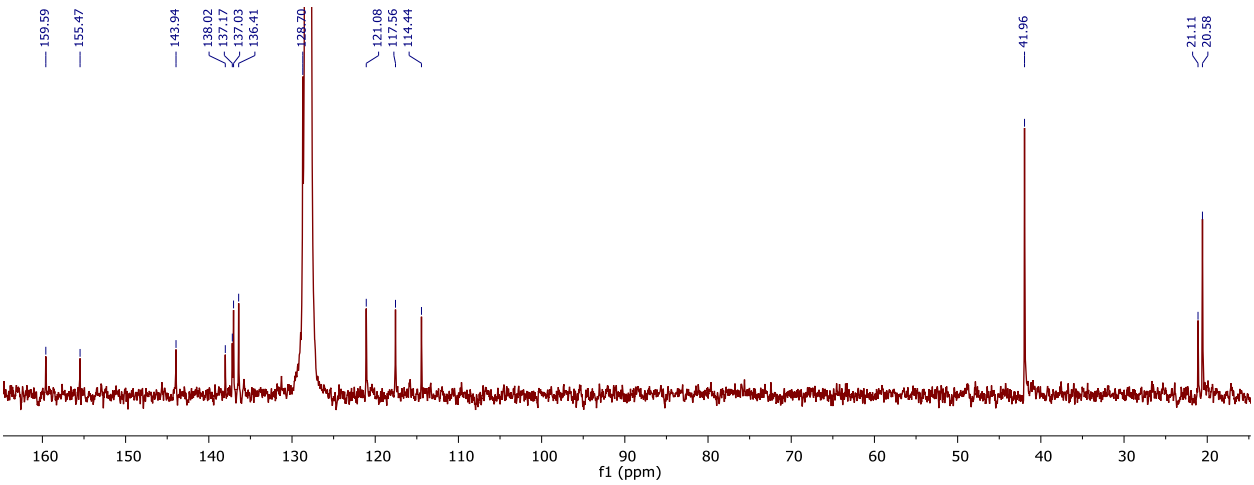

Figure S30. ^{13}C NMR spectrum of **18** in C_6D_6.

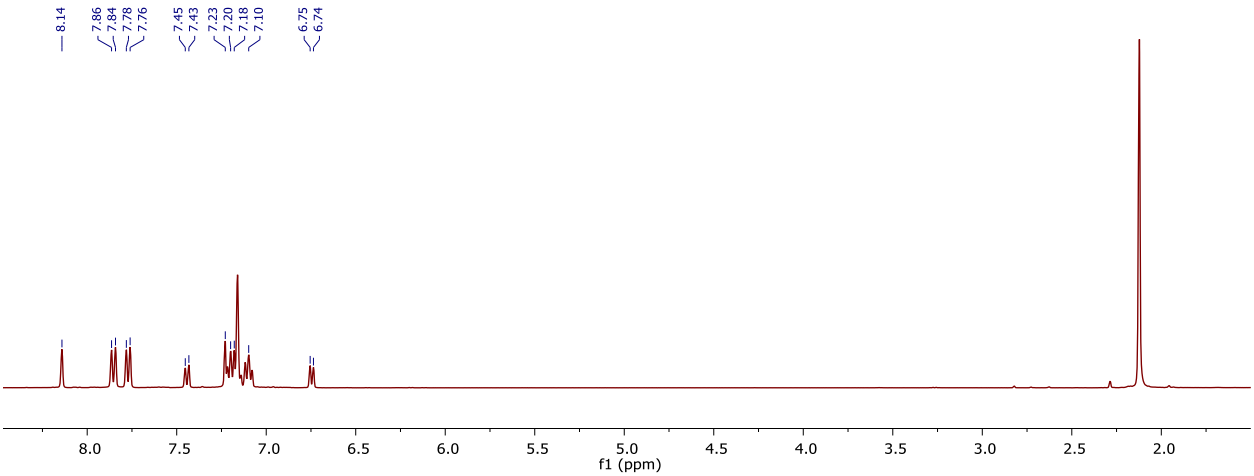

Figure S31. ^{1}H NMR spectrum of **19** in C_6D_6.

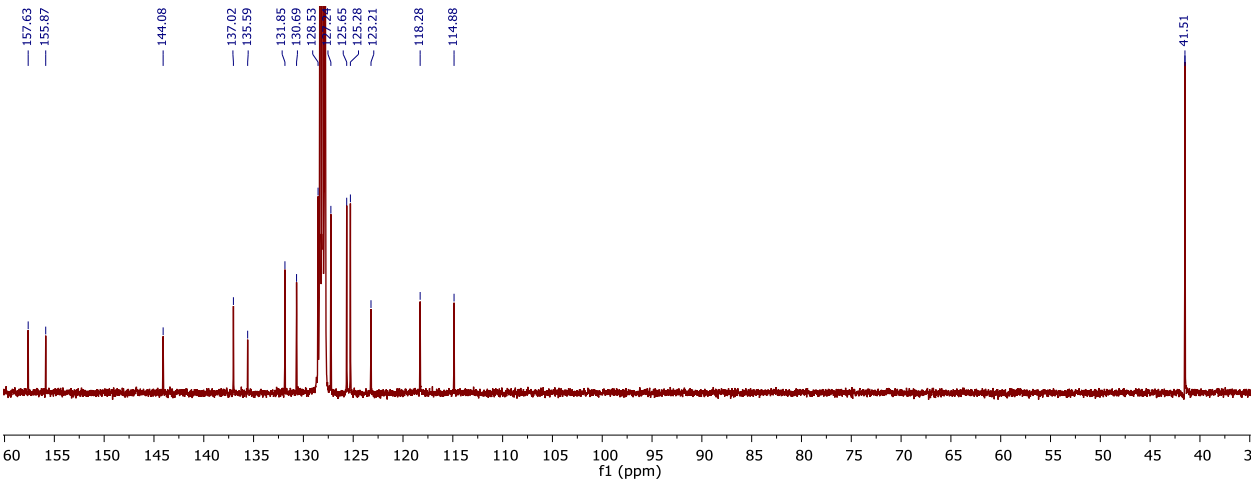

Figure S32. ^{13}C NMR spectrum of **19** in C_6D_6.

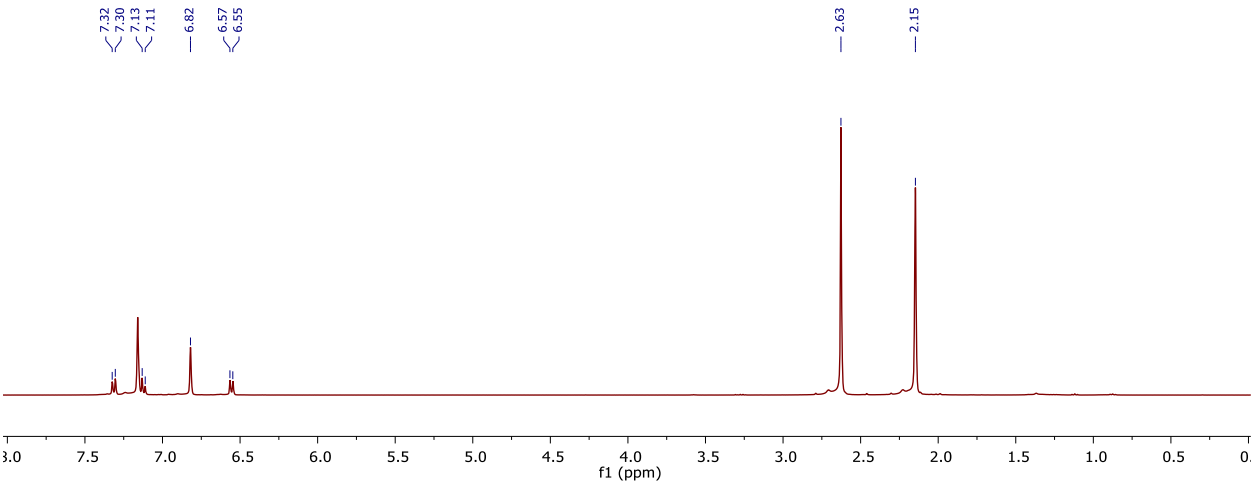

Figure S33. ^{1}H NMR spectrum of **20** in C_6D_6.

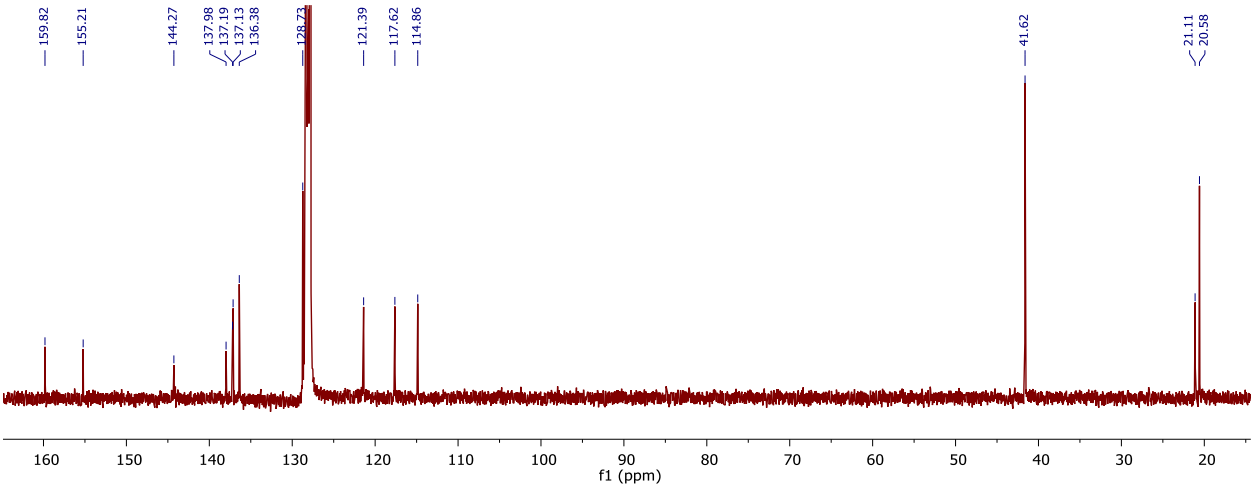

Figure S34. ^{13}C NMR spectrum of **20** in C_6D_6.

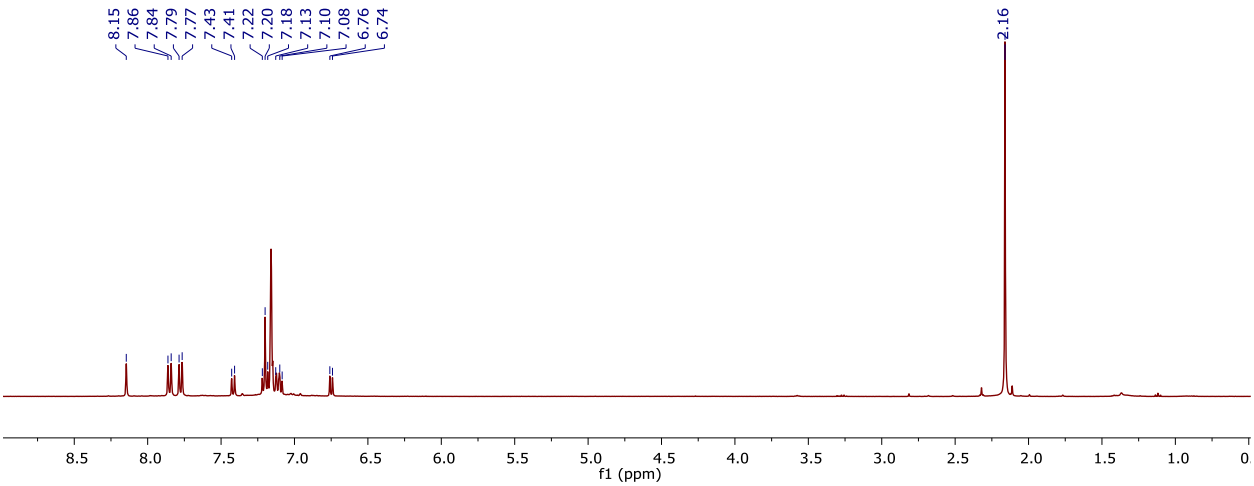

Figure S35. ^{1}H NMR spectrum of **21** in C_6D_6.

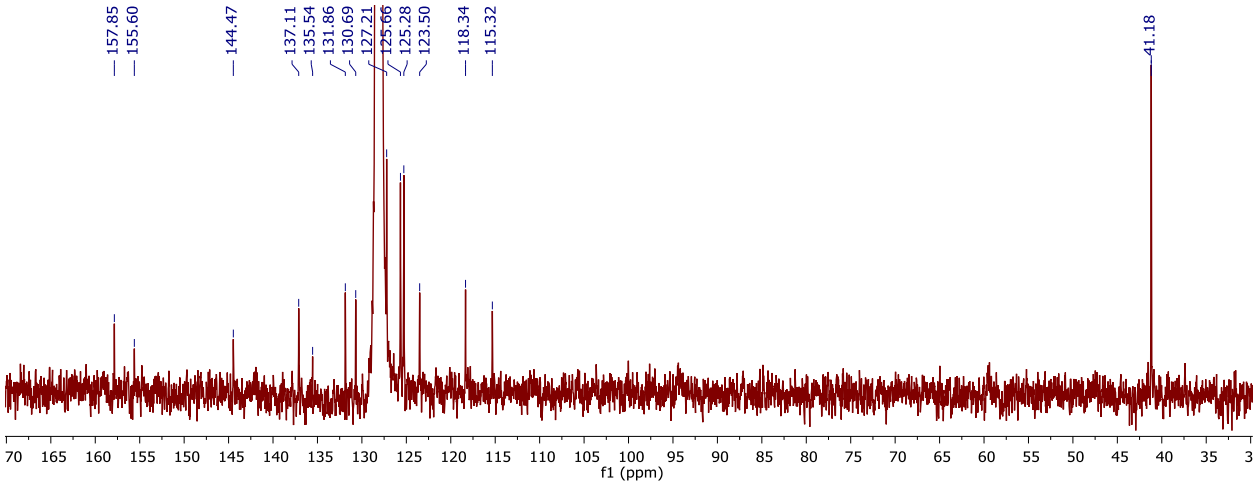

Figure S36. ^{13}C NMR spectrum of **21** in C_6D_6.

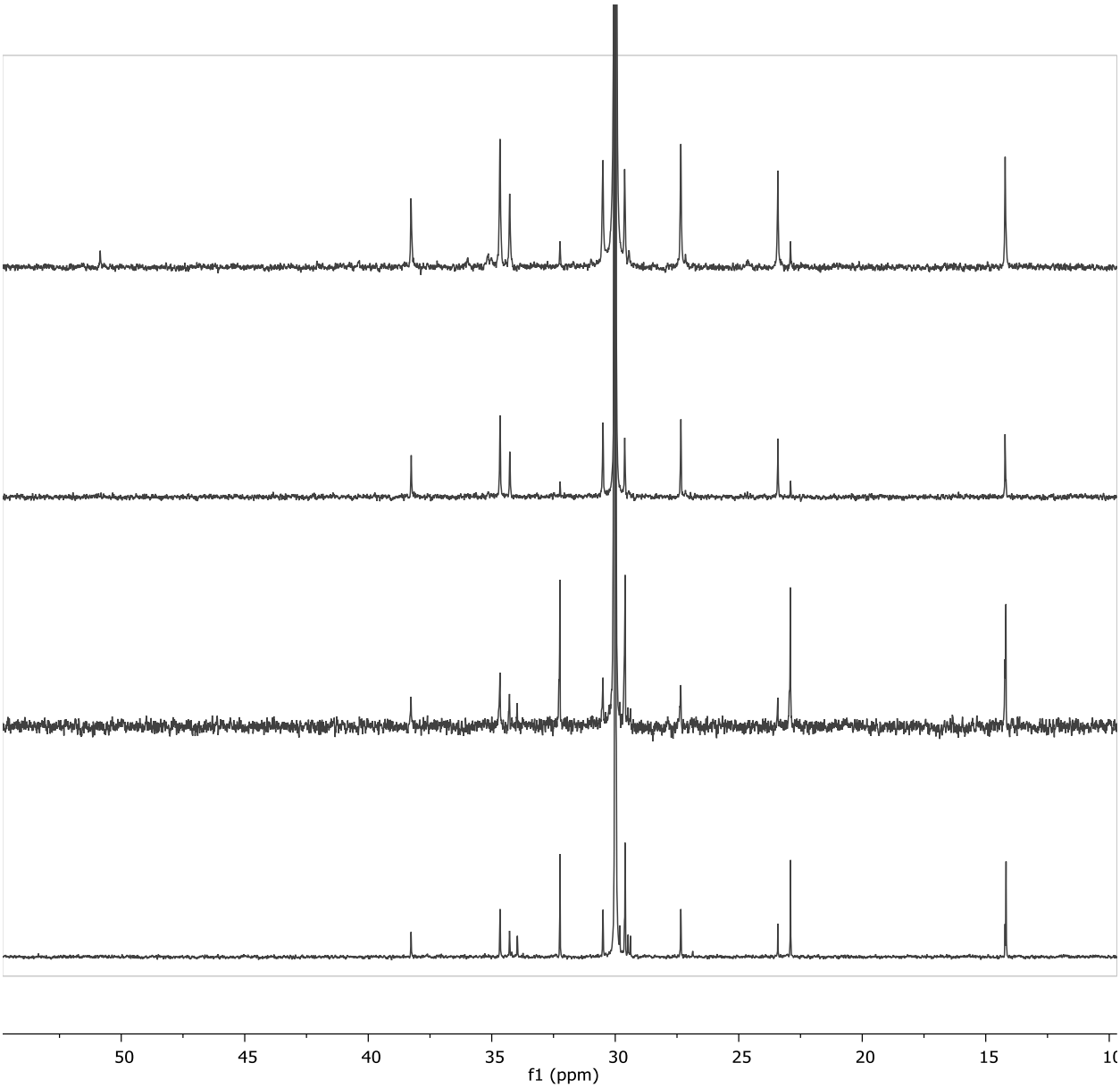

Figure S37. ^{13}C NMR spectra of ethylene-1-hexene copolymers from **16**, **17**, **18**, and **19** in $C_2D_2Cl_4$ at 130 ^{o}C.

Complete Polymer Tables

Table S1. Complete small-scale ethylene polymerization results.

	M	Ar	Time	Yield	Activity	M_W[a]	M_W/M_N [b]	T_M[c]	χ_c[d]
			min	g	g $mmol_m^{-1}$ h^{-1}	kDa		°C	%
1[e]	Zr	Mes	30	0.06	--	n.d.[f]	n.d.		
2[g]	Zr	Mes	30	0.20	100	185	155		
3	Zr	Mes	30	1.47	740	94	126	124.2	65.3
4	Zr	Mes	10	0.49	730	93	130		
5	Zr	Mes	10	0.31	460	65	87	124.7	71.1
6	Zr	Mes	10	0.31	460	141	188		
7	Zr	Anth	10	0.08	120	81	93	126.4	72.5
8	Zr	Anth	30	0.72	360	110	145	125.6	74.5
9	Zr	Anth	30	0.82	410	191	260		
10	Hf	Mes	30	0.006	--	n.d.	n.d.		
11[h]	Ti	Mes	3.5	0.33	1400	355	143		
12	Ti	Mes	1	0.23	3400	293	130		
13	Ti	Mes	1	0.24	3600	271	141	134.5	75.4
14[i]	Ti	Mes	8	0.17	3000	917	143	134.8	58.1
15	Ti	Anth	1	0.23	3400	255	112	135.6	72.7
16	Ti	Anth	1	0.22	3400	286	130	134.1	68.8
17[i]	Ti	Anth	10	0.12	3000	1069	91	133.5	56.3

Conditions: 100 PSI, 10 mL PhCl, 200 equiv. $AlMe_3$, 3 equiv. $[CPh_3][B(C_6F_5)_4]$. [a]From GPC analysis; [b]From GPC analysis; [c]Melting temperature determined by DSC; [d]Percent crystallinity determined by DSC; [e]1000 equiv. of MMAO and PhMe was used in place of the $AlMe_3/[CPh_3][B(C_6F_5)_4]$ activator mixture and PhCl; [f]Not determined; [g]1000 equiv. of MMAO was used in place of the $AlMe_3/[CPh_3][B(C_6F_5)_4]$ activator mixture; [h]Stirring lost over the course of the reaction due to high viscosity; [i]0.4 μmol precatalyst loading.

Table S2. Complete ethylene-1-hexene copolymerization results.

	M	**Ar**	**Time**	**Yield**	**Activity**	**M_W**[a]	**M_W/ M_N** [b]	**% I**[c]	**T_M**[d]	**χ_C**[e]
			min	g	g $mmol_M^{-1}$ h^{-1}	kDa			°C	%
1	Zr	Mes	10	0.75	1100	2.5	4.1	n.d.	119.9	50.09
2	Zr	Mes	10	0.45	680	84.1	107.0	1.3	122.4	61.18
3	Zr	Anth	10	0.14	200	63.0	74.0	1.0	123.3	58.58
4	Zr	Anth	30	0.30	150	221.2	207.1	n.d.	125.7	64.1
5	Zr	Anth	30	1.18	590	116.9	149.9	n.d.	122.6	52.88
6	Ti	Mes	1	0.33	5000	271.9	136.8	n.d.	120.0	31.55
7	Ti	Mes	1	0.39	5900	197.2	73.4	2.2	121.3	32.73
8	Ti	Anth	2	0.30	2300	530.6	204.2	n.d.	121.4	33.82
9	Ti	Anth	1	0.27	4000	322.9	109.5	1.6	120.3	32.66

Conditions: 100 PSI, 10 mL PhCl, 200 equiv. $AlMe_3$, 3 equiv. $[CPh_3][B(C_6F_5)_4]$, 1000 equiv. 1-hexene.

[a]From GPC analysis; [b]From GPC analysis; [c]Insertion mol% as determined by integration of the ^{13}C NMR; [d]Melting temperature determined by DSC; [e]Percent crystallinity determined by DSC.

Table S3. Complete large-scale ethylene and ethylene-1-hexene polymerization results

	M	Ar	Comonomer	T	Yield	Activity	T_m[a]	χ_c[b]	Mw[c]	M_W/M_N[d]
				°C	g	g $mmol_M^{-1}$ h^{-1}	°C	%	kDa	
1	Zr	Mes	-	60	1.53	153	132.6	82.25	182	89.0
2	Zr	Mes	1-hexene	60	0.6	60	124.6	53.06	109	60.0
3	Zr	Mes	-	80	1.4	140	132.1	75.37	72	47.7
4	Zr	Mes	1-hexene	80	0.7	70	122.7	57.17	20	15.1
5	Ti	Mes	-	60	2.1	210	137.6	76.65	316	31.4
6	Ti	Mes	1-hexene	60	3.5	350	118.8	32.21	156	14.2
7	Ti	Mes	-	80	4.9	490	134.3	81.81	154	14.6
8[e]	Ti	Mes	-	80	1.1	110	135.8	53.23	1,000	4.3
9	Ti	Mes	1-hexene	80	4.4	440	118.5	27.62	79	10.8
10	Hf	Mes	-	60	0.056	5.6	135.2	63.97	130	16.7
11	Hf	Mes	-	80	0.028	2.8	134.4	63.39	201	32.3
12	Zr	Anth	-	80	0.6	60	129.7	72.31	389	129.0
13	Zr	Anth	1-hexene	80	0.1	10	126.1	62.06	165	51.3

Conditions: 10 μmol precatalyst, 5 bar ethylene pressure, 1000 equiv. MAO, 0 or 20 mL 1-hexene, 100 mL toluene. [a]Melting temperature determined by DSC; [b]Percent crystallinity determined by DSC; [c]Determined by GPC; [d]Determined by GPC where PDI = M_W/M_N; [e]500 equiv. BHT.

GPC Traces

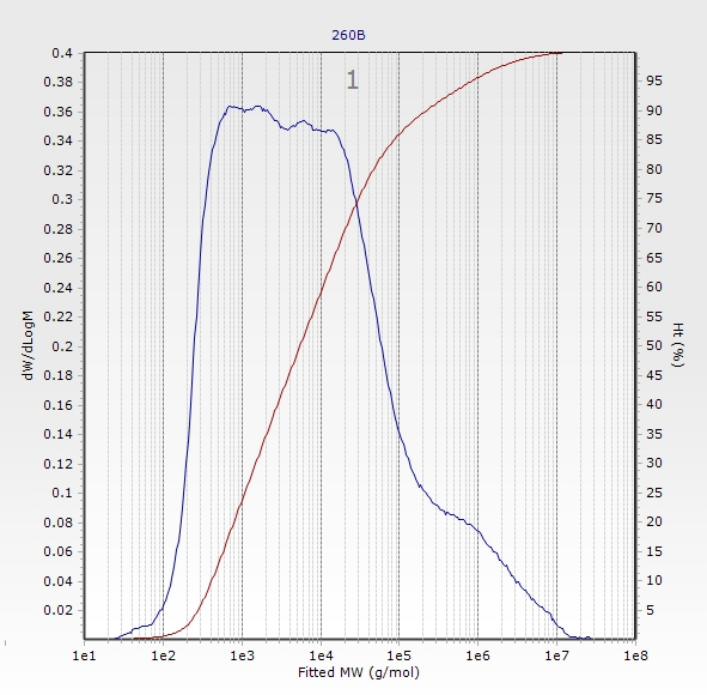

Figure S38. GPC trace from the ethylene polymerization by **(DPP^{mes})Zr(NMe$_2$)$_3$** using 1000 equiv. MMAO at 100 PSI ethylene in PhCl.

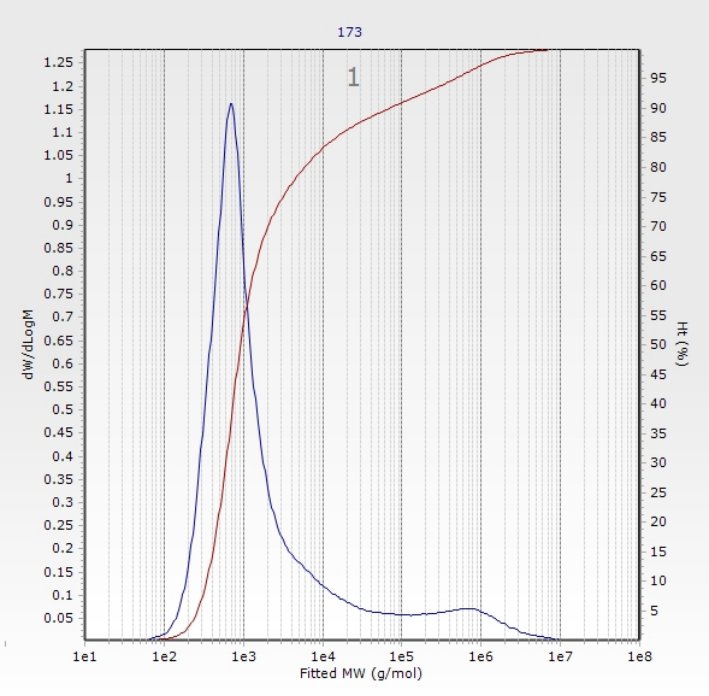

Figure S39. GPC trace from the ethylene polymerization by **(DPP^{mes})Zr(NMe$_2$)$_3$** using 200 equiv. AlMe$_3$ and 3 equiv. [CPh$_3$][B(C$_6$F$_5$)$_4$] at 100 PSI ethylene in PhCl over 30 min.

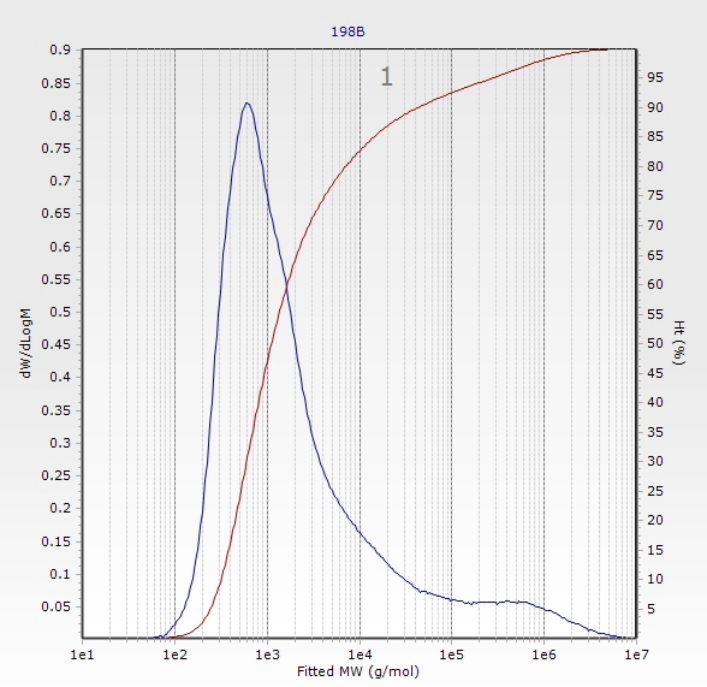

Figure S40. GPC trace from the ethylene polymerization by **(DPP^{mes})Zr(NMe$_2$)$_3$** using 200 equiv. AlMe$_3$ and 3 equiv. [CPh$_3$][B(C$_6$F$_5$)$_4$] at 100 PSI ethylene in PhCl over 10 min.

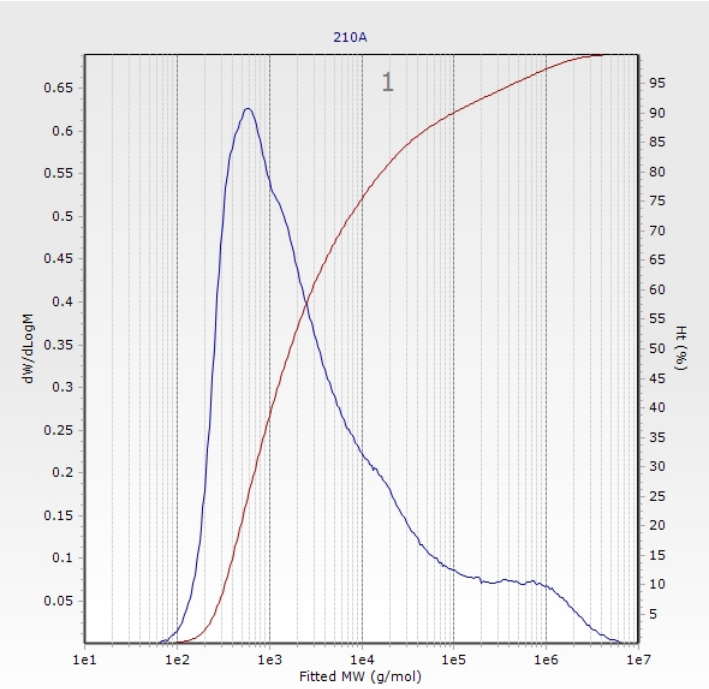

Figure S41. GPC trace from the ethylene polymerization by **(DPP^{anth})Zr(NMe$_2$)$_3$** using 200 equiv. AlMe$_3$ and 3 equiv. [CPh$_3$][B(C$_6$F$_5$)$_4$] at 100 PSI ethylene in PhCl over 10 min.

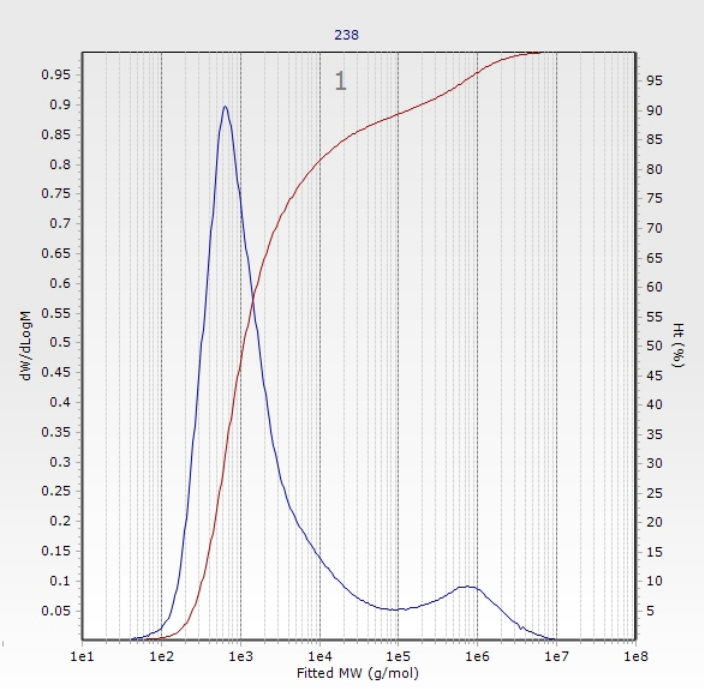

Figure S42. GPC trace from the ethylene polymerization by **(DPP^{anth})Zr(NMe$_2$)$_3$** using 200 equiv. AlMe$_3$ and 3 equiv. [CPh$_3$][B(C$_6$F$_5$)$_4$] at 100 PSI ethylene in PhCl over 30 min.

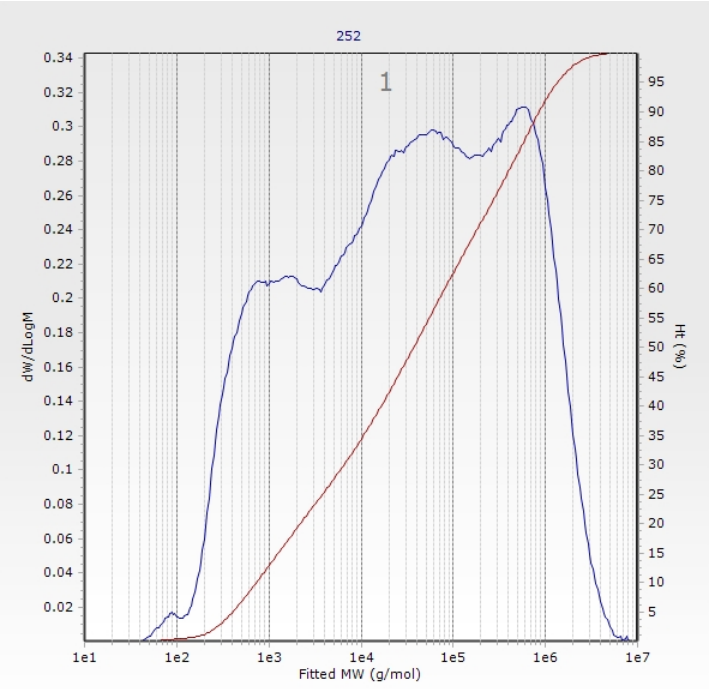

Figure S43. GPC trace from the ethylene polymerization by **(DPP^{mes})Ti(NMe$_2$)$_3$** using 4.0 μmol precatalyst, 200 equiv. AlMe$_3$ and 3 equiv. [CPh$_3$][B(C$_6$F$_5$)$_4$] at 100 PSI ethylene in PhCl over 1 min.

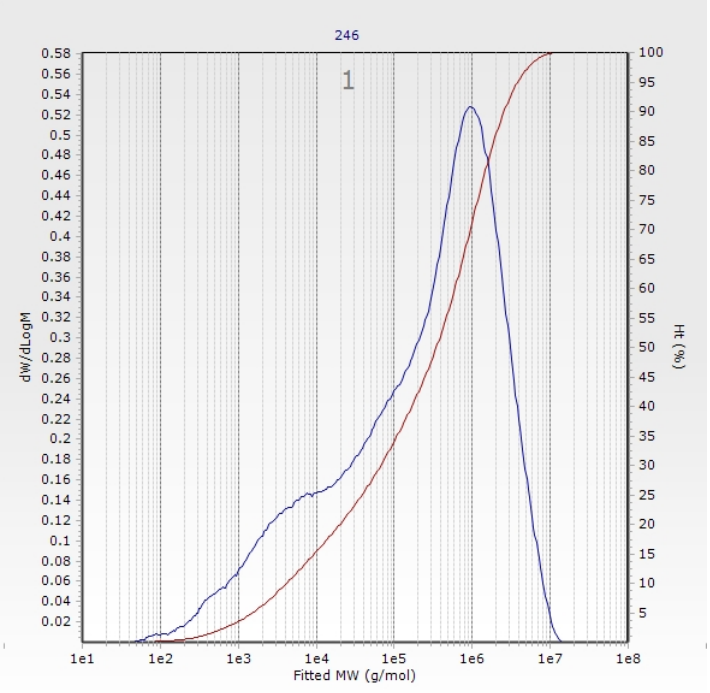

Figure S44. GPC trace from the ethylene polymerization by **(DPP^{mes})Ti(NMe$_2$)$_3$** using 0.40 μmol precatalyst, 200 equiv. $AlMe_3$ and 3 equiv. $[CPh_3][B(C_6F_5)_4]$ at 100 PSI ethylene in PhCl over 8 min.

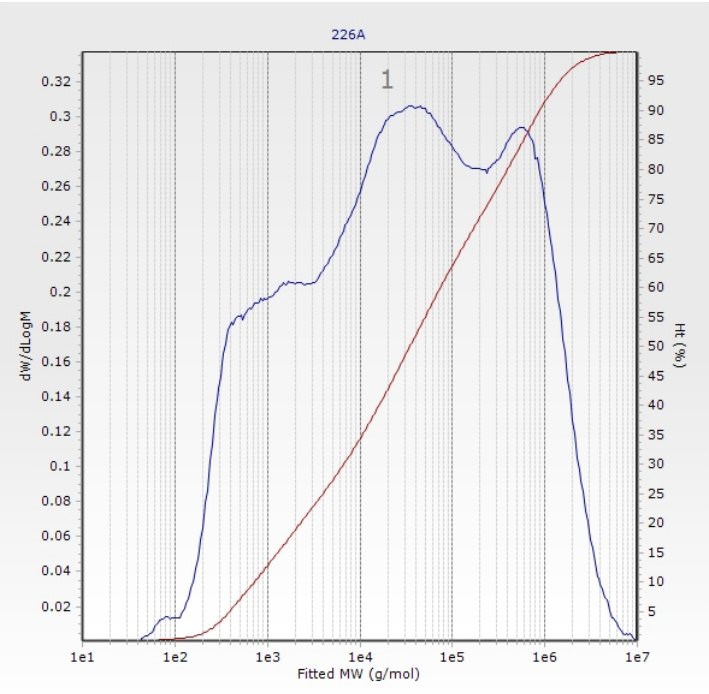

Figure S45. GPC trace from the ethylene polymerization by **(DPP^{anth})Ti(NMe$_2$)$_3$** using 4.0 μmol precatalyst, 200 equiv. $AlMe_3$ and 3 equiv. $[CPh_3][B(C_6F_5)_4]$ at 100 PSI ethylene in PhCl over 1 min.

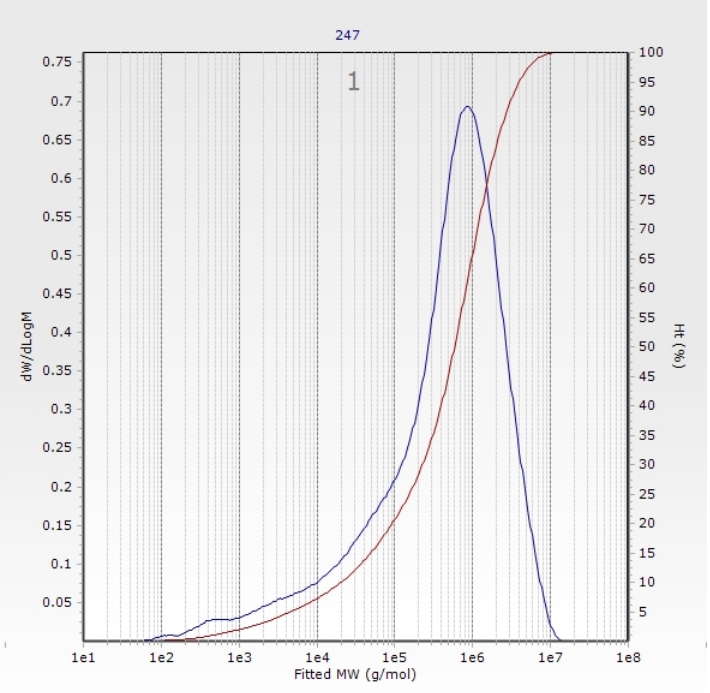

Figure S46. GPC trace from the ethylene polymerization by **(DPP^{anth})Ti(NMe$_2$)$_3$** using 0.40 μmol precatalyst, 200 equiv. $AlMe_3$ and 3 equiv. $[CPh_3][B(C_6F_5)_4]$ at 100 PSI ethylene in PhCl over 10 min.

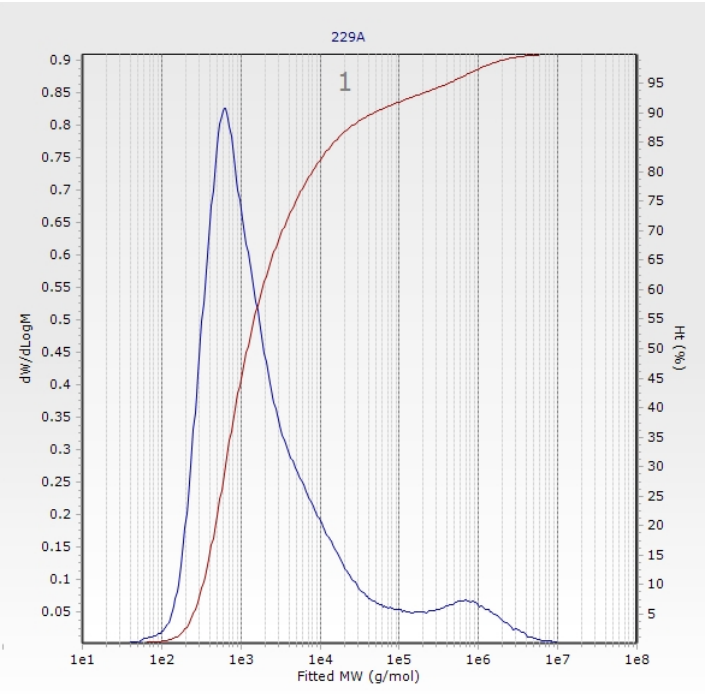

Figure S47. GPC trace from the ethylene-1-hexene copolymerization by **(DPP^{mes})Zr(NMe$_2$)$_3$** using 1000 equiv. 1-hexene 200 equiv. $AlMe_3$ and 3 equiv. $[CPh_3][B(C_6F_5)_4]$ at 100 PSI ethylene in PhCl over 10 min.

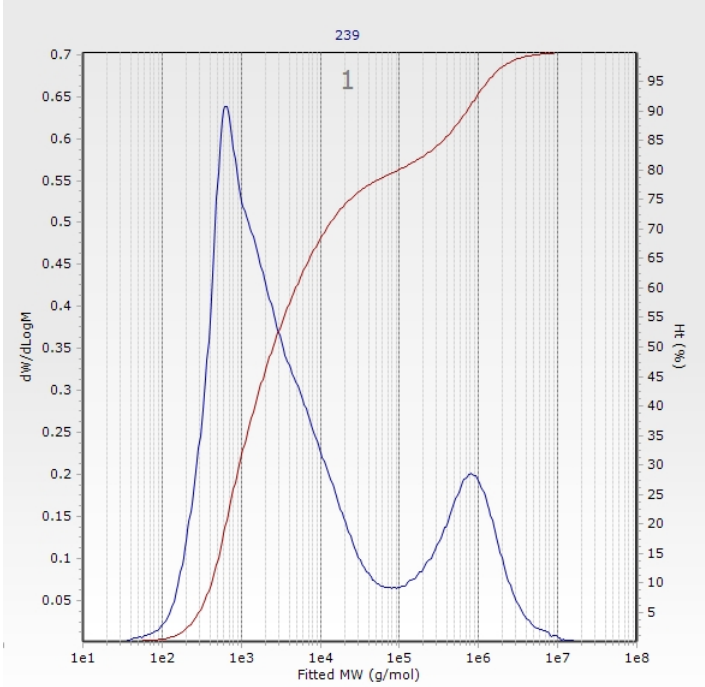

Figure S48. GPC trace from the ethylene-1-hexene copolymerization by **(DPP^{anth})Zr(NMe$_2$)$_3$** using 1000 equiv. 1-hexene 200 equiv. $AlMe_3$ and 3 equiv. $[CPh_3][B(C_6F_5)_4]$ at 100 PSI ethylene in PhCl over 10 min.

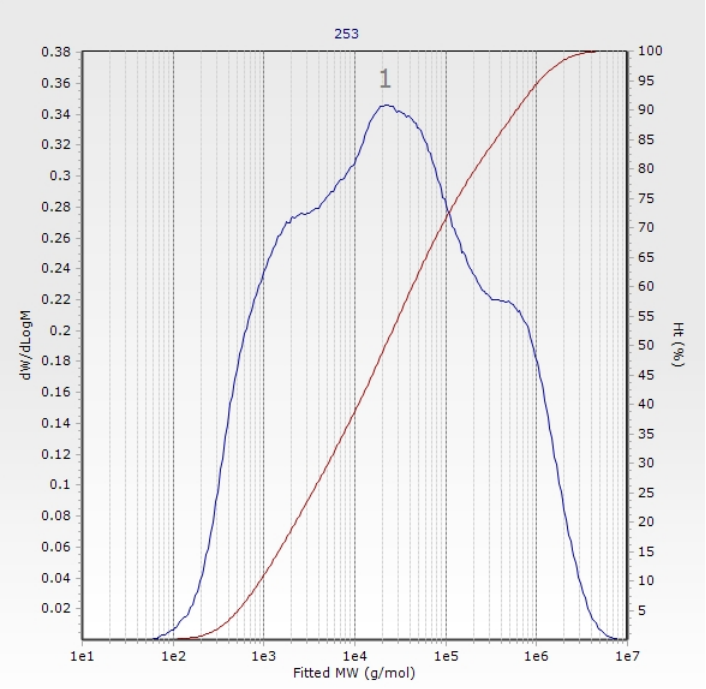

Figure S49. GPC trace from the ethylene-1-hexene copolymerization by **(DPP^{mes})Ti(NMe$_2$)$_3$** using 1000 equiv. 1-hexene 200 equiv. $AlMe_3$ and 3 equiv. $[CPh_3][B(C_6F_5)_4]$ at 100 PSI ethylene in PhCl over 10 min.

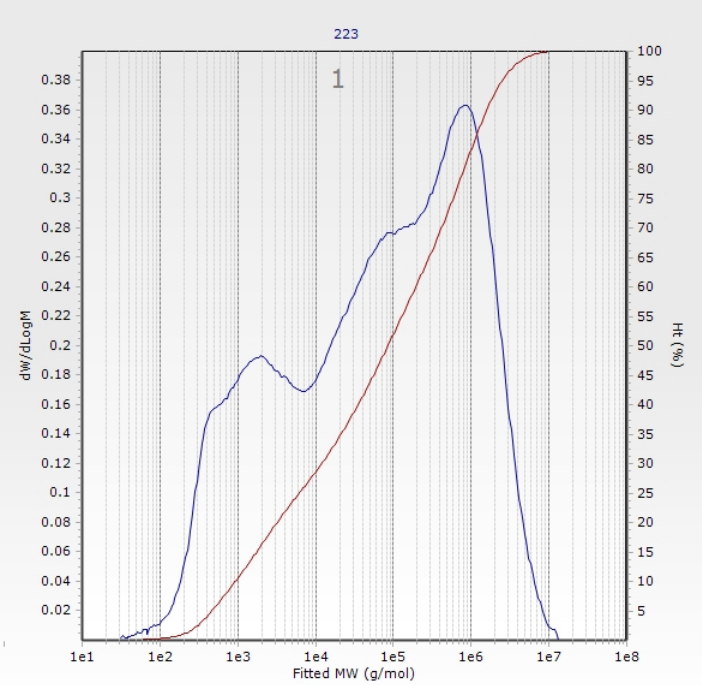

Figure S50. GPC trace from the ethylene-1-hexene copolymerization by **(DPP^{anth})Ti(NMe$_2$)$_3$** using 1000 equiv. 1-hexene 200 equiv. $AlMe_3$ and 3 equiv. $[CPh_3][B(C_6F_5)_4]$ at 100 PSI ethylene in PhCl over 10 min.

Further Discussion of Polymer GPC Data and Activation Modes

Very broad, multimodal molecular weight distributions were observed by GPC for complexes **16**, **17**, **18**, and **19** using either MMAO-12 or $AlMe_3$/$[CPh_3][B(C_6F_5)_4]$. NMR analysis of the ethylene homopolymers from **18** and **19** showed no evidence of branching, though methyl-terminated chains could be clearly observed. Resonances corresponding to terminal olefins were observed by ^1H NMR, consistent with some chain termination by β-hydride elimination. Integration of the olefinic and methyl signals shows a relative ratio of 1:9.40 indicating that the majority of polymer chains are methyl terminated at both ends. This suggests that chain transfer to Al may be the dominant mode of chain termination, potentially leading to the observed broadened molecular weight distributions.[1,2] Another possible explanation for the broadened molecular weight distributions is the formation of a variety of species competent for ethylene oligomerization and polymerization under catalysis conditions, depending on the DPP binding mode, degree of metal alkylation, and aluminum coordination of potential free pyridine arms.[3] Ethylene polymerization from **16** and MAO was also run in the presence of BHT (0.5 equiv. relative to MAO) as a free $AlMe_3$ scavenger (Table S3, Entry 8).[4] In comparison with ethylene polymerization using **16** under otherwise identical conditions (Table S3, Entry 7), a substantially higher molecular weight and lower M_W/M_N is observed (M_W of 1000 kDa and M_W/M_N of 4.3 vs. M_W of 155 and M_W/M_N of 15). These results are consistent with the proposal that chain transfer to aluminum is the dominant mode of chain termination.

Crystallographic Information

Refinement Details: Crystals were mounted on a glass fiber or MiTeGen loop using Paratone oil, then placed on the diffractometer under a nitrogen stream. Diffractometer manipulations, including data collection, integration, and scaling were performed using the Bruker APEXII software.[5] Absorption corrections were applied using SADABS or TWINABS (**8** and **14**).[6] Space groups were determined on the basis of systematic absences and intensity statistics and the structures were solved in the Olex 2 software interface[7] by intrinsic phasing using XT (incorporated into SHELXTL)[8] and refined by full-matrix least squares on F^2. All non-hydrogen atoms were refined using anisotropic displacement parameters, except as noted. Hydrogen atoms were placed in the idealized positions and refined using a riding model. Graphical representation of structures with 50% probability thermal ellipsoids were generated using Diamond 3 visualization software.[9] Disordered solvents of crystallization were observed in the difference maps of **12** and **15**; these were removed using the solvent mask tool in Olex 2[7, 10] as they could not be satisfactorily modeled.

Table S4. Crystal and refinement data for **8**, **11**, and **12**

	8	**11**	**12**
CCDC Number	1901334	1901318	1900723
Empirical formula	$C_{53}H_{57}N_5Si_4Y$	$C_{36}H_{40}AlN_3$	$C_{76}H_{96}N_3OSi_4Y$
Formula weight	965.30	541.69	1268.83
T (K)	100	100	100
a, Å	12.8334(15)	10.0846(7)	11.597(5)
b, Å	18.935(2)	10.7246(7)	16.582(7)
c, Å	21.972(2)	14.7495(11)	21.396(5)
α, °	66.153(4)	88.535(3)	96.041(6)
β, °	86.673(4)	85.525(3)	104.761(6)
γ, °	89.451(4)	72.732(3)	94.927(7)
Volume, Å^3	4874.6(10)	1518.66(19)	3929(3)
Z	4	2	2
Crystal system	Triclinic	Triclinic	Triclinic
Space group	P -1	P -1	P -1
θ range, °	2.347 to 25.702	2.419 to 27.463	2.297 to 27.387
μ, mm^{-1}	1.336	0.096	0.845
Abs. Correction	Multi-scan	Multi-scan	Multi-scan
GOF	1.124	1.046	1.042
R_1,[a] wR_2 [b] [I>2 σ(I)]	0.0497, 0.1431	0.0622, 0.1750	0.0532, 0.1554
Radiation Type	Mo Kα	Mo Kα	Mo Kα

[a] $R1 = \sum||F_o| - |F_c||/\sum|F_o|$. [b] $wR2 = [\sum[w(F_o^2 - F_c^2)^2]/\sum[w(F_o^2)^2]]^{1/2}$.

Table S5. Crystal and refinement data for **14**, **3.19**, and **3.20**

	14	**15**	**16**
CCDC Number	1900722	1900724	1900725
Empirical formula	$C_{80}H_{78}N_5Si_2Y$	$C_{42}H_{26}Cl_3N_3Zr$	$C_{38}H_{48}N_6Ti$
Formula weight	1254.57	770.23	636.72
T (K)	100	100	100
a, Å	12.1287(7)	13.1280(6)	13.9945(10)
b, Å	22.4625(13)	20.0709(9)	14.8672(11)
c, Å	24.6736(14)	16.0162(7)	17.6684(12)
α, °	90	90	73.736(3)
β, °	90.137(3)	110.871(2)	87.627(3)
γ, °	90	90	88.402(3)
Volume, Å^3	6722.1(7)	3943.22	3525.4(4)
Z	4	4	4
Crystal system	Monoclinic	Monoclinic	Triclinic
Space group	P $2_1/n$	P $2_1/c$	P -1
d_{calc}, g/cm$_3$	1.240	1.297	1.200
θ range, °	3.936 to 79.873	2.439 to 27.4795	2.403 to 27.487
μ, mm^{-1}	1.925	0.513	0.277
Abs. Correction	Multi-scan	Multi-scan	Multi-scan
GOF	1.023	1.040	1.035
R_1, [a] wR_2 [b] [I>2 σ(I)]	0.0421, 0.1080	0.0247, 0.0686	0.0336, 0.0901
Radiation Type	Cu Kα	Mo Kα	Mo Kα

[a] $R1 = \sum||F_o| - |F_c||/\sum|F_o|$. [b] $wR2 = [\sum[w(F_o^2 - F_c^2)^2]/\sum[w(F_o^2)^2]]^{1/2}$.

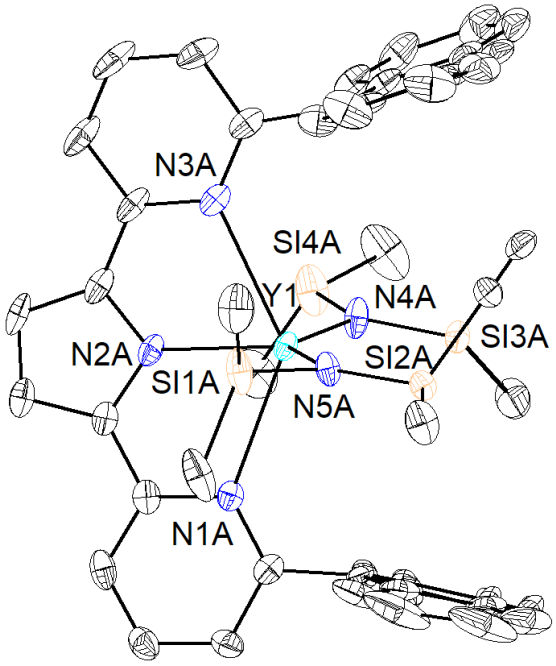

Figure S51. Structural drawing of **8** with 50% probability anisotropic displacement ellipsoids. Hydrogen atoms are omitted for clarity. One of two molecules in the asymmetric unit is shown for clarity. The major populations of the disordered tetramethyldisilylazide groups are shown for clarity.

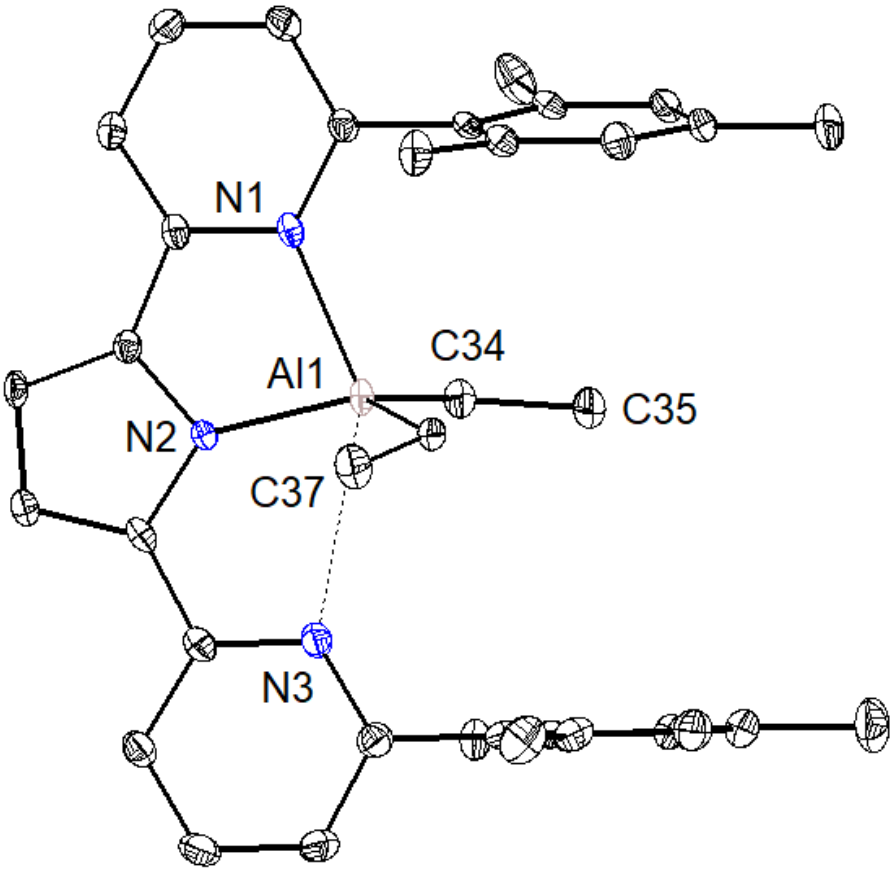

Figure S52. Structural drawing of **11** with 50% probability isotropic displacement ellipsoids. Hydrogen atoms are omitted for clarity.

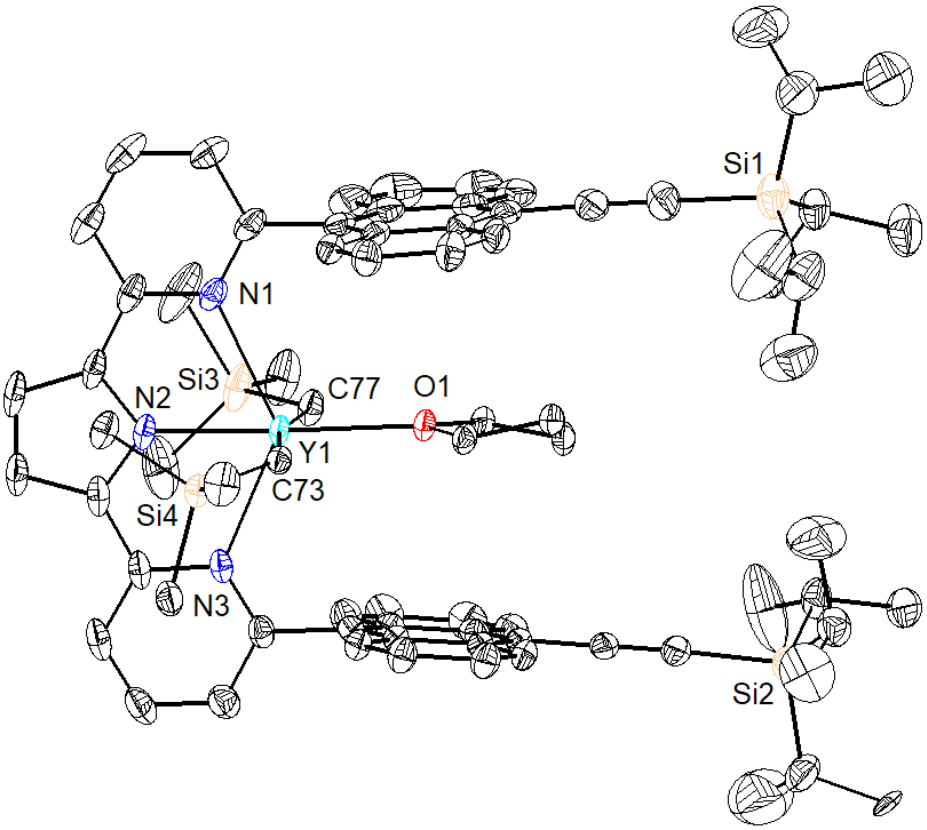

Figure S53. Structural drawing of **12** with 50% probability anisotropic displacement ellipsoids. Hydrogen atoms are omitted for clarity. The major population of the disordered *iso*-propyl group is shown for clarity.

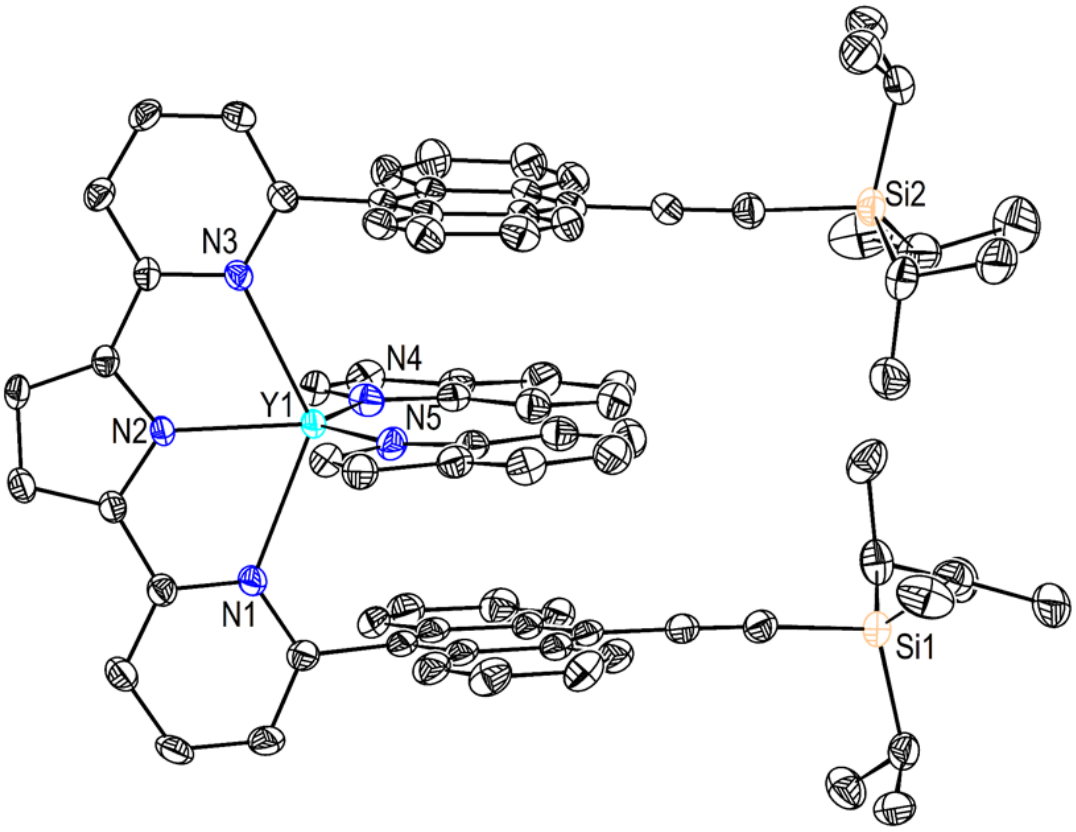

Figure S54. Structural drawing of **14** with 50% probability anisotropic displacement ellipsoids. Hydrogen atoms are omitted for clarity.

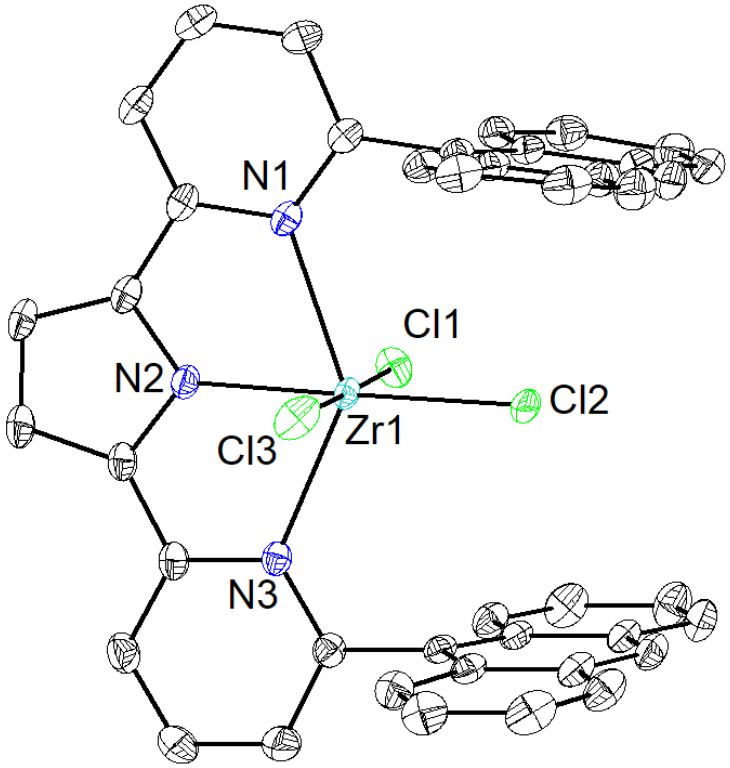

Figure S55. Structural drawing of **(DPP^{anth})ZrCl$_3$** with 50% probability anisotropic displacement ellipsoids. Hydrogen atoms are omitted for clarity.

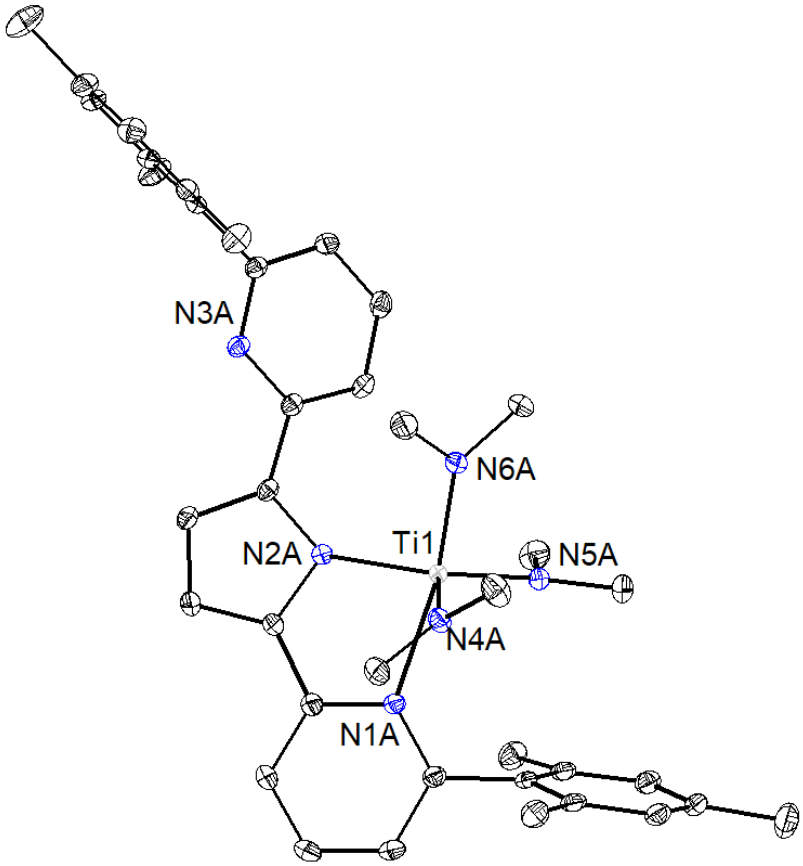

Figure S56. Structural drawing of **(DPP^{mes})Ti(NMe$_2$)$_3$** with 50% probability anisotropic displacement ellipsoids. Hydrogen atoms are omitted for clarity. One of two molecules in the asymmetric unit is shown for clarity.

References

1. Britovsek, G. J. P.; Bruce, M.; Gibson, V. C.; Kimberley, B. S.; Maddox, P. J.; Mastroianni, S.; McTavish, S. J.; Redshaw, C.; Solan, G. A.; Strömberg, S.; White, A. J. P.; Williams, D. J. Iron and Cobalt Ethylene Polymerization Catalysts Bearing 2,6-Bis(Imino)Pyridyl Ligands: Synthesis, Structures, and Polymerization Studies. *J. Am. Chem. Soc.* **1999**, *121*, 8728-8740.

2. (a) Nakazawa, H.; Ikai, S.; Imaoka, K.; Kai, Y.; Yano, T. Polymerization of olefins with titanium and zirconium complexes containing hydrotris(pyrazolyl)borate of hydrotris(3,5-dimethylpyrazolyl)borate. *J. Mol. Cat. A* **1998**, *132*, 33-41; (b) Scollard, J. D.; McConville, D. H.; Vittal, J. J.; Payne, N. C. Chelating diamide complexes of titanium: new catalyst precursors for the highly active and living polymerization of alpha-olefins. *J. Mol. Cat. A* **1998**, *128*, 201-214; (c) Murtuza, S.; Jr., O. L. C.; Jordan, R. F. Ethylene Polymerization Behavior of Tris(pyrazolyl)borate Titanium(IV) Complexes. *Organometallics* **2002**, *21*, 1882-1890; (d) Amin, S. B.; Marks, T. J. Versatile pathways for in situ polyolefin functionalization with heteroatoms: catalytic chain transfer. *Angew. Chem. Int. Ed.* **2008**, *47*, 2006-2025; (e) Chan, M. C. W.; Tam, K.-H.; Zhu, N.; Chiu, P.; Matsui, S. Synthesis, Structures, and Olefin Polymerization Characteristics of Group 4 Catalysts [Zr{$(OAr)_2$py}Cl_2(D)] (D = O-Donors, Cl[HPR_3]) Supported by Tridentate Pyridine-2,6-bis(aryloxide) Ligands. *Organometallics* **2006**, *25*, 785-792; (f) Saito, J.; Tohi, Y.; Matsukawa, N.; Mitani, M.; Fujita, T. Selective Synthesis of Al-Terminated Polyethylenes Using a Bis(Phenoxy-Imine)Zr Complex with Methylalumoxane. *Macromolecules* **2005**, *38*, 4955-4957; (g) Michiue, K.; Jordan, R. F. Comparison of Olefin Polymerization Behavior of Catalysts Generated by MAO Activation of Ti^{III} and Ti^{IV} Tris(pyrazolyl)borate Complexes. *Macromolecules* **2003**, *36*, 9707-9709; (h) Tohi, Y.; Mako, H.; Matsui, S.; Onda, M.; Fujita, T. Polyethylenes with Uni-, Bi-, and Trimodal Molecular Weight Distributions Produced with a Single Bis(phenoxy−imine)zirconium Complex. *Macromolecules* **2003**, *36*, 523-525; (i) Obenauf, J.; Kretschmer, W. P.; Kempe, R. Efficient Synthesis of Aluminium-Terminated Polyethylene by Means of Irreversible Coordinative Chain-Transfer Polymerisation Using a Guanidinatotitanium Catalyst. *Eur. J. Inorg. Chem.* **2014**, *2014*, 1446-1453; (j) Lee, J.; Kim, Y. Preparation of polyethylene with controlled bimodal molecular weight distribution using zirconium complexes. *J. Industrial Eng. Chem.* **2012**, *18*, 429-432; (k) Park, S.-J.; Han, Y.-G.; Kim, S.-K.; Lee, J.-S.; Kim, H.-K.; Do, Y.-K. Synthesis and Polymerization Behavior of Cp*Ti(2-pyridinecarboxylato)$_2$Cl: A New Cp/non-Cp Hybrid Catalyst for Polyethylene with Multimodal Molecular Weight Distribution. *Bull. Korean Chem. Soc.* **2005**, *26*, 713-714; (l) Resconi, L.; Piemontesi, F.; Franciscono, G.; Abis, L.; Fiorani, T. Olefin polymerization at bis(pentamethylcyclopentadienyl)zirconium and -hafnium centers: chain transfer mechanisms. *J. Am. Chem. Soc.* **1992**, *114*, 1025-1032; (m) Mogstad, A. L.; Waymouth, R. M. Chain transfer to aluminum in the homogeneous cyclopolymerization of 1,5-hexadiene. *Macromolecules* **1992**, *25*, 2282-2284; (n) Rieger, B.; Reinmuth, A.; Röll, W.; Brintzinger, H. H. Highly isotactic polypropene prepared with rac-dimethylsilyl-bis(2-methyl-4-*t*-butyl-cyclopentadienyl) zirconiumdichloride: An NMR investigation of the polymer microstructure. *J. Mol. Cat.* **1993**, *82*, 67-73; (o) Leino, R.; Luttikhedde, H. J. G.; Lehmus, P.; Wilén, C.-E.; Sjöholm, R.; Lehtonen, A.; Seppälä, J. V.; Näsman, J. H. Homogeneous α-Olefin Polymerizations over Racemic Ethylene-Bridged *ansa*-Bis(2-(*tert*-butyldimethylsiloxy)- 1-indenyl) and *ansa*-Bis(2-(*tert*-butyldimethylsiloxy)- 4,5,6,7-tetrahydro-1-indenyl) Metallocene Dichlorides. *Macromolecules* **1997**, *30*, 3477-3483; (p) Valente, A.; Mortreux, A.; Visseaux, M.; Zinck, P. Coordinative Chain Transfer Polymerization. *Chem. Rev.* **2013**, *113*, 3836-3857; (q) Byun, D.-J.; Shin, D.-K.; Kim, S. Y. Chain transfer reactions in metallocene catalyzed polymerization of allylbenzene. *Polym. Bull.* **1999**, *42*, 301-307; (r) Byun, D.-J.; Shin, D.-K.; Kim, S. Y. Copolymerization of ethylene with allylbenzene using *rac*-

ethylenebis(indenyl)zirconium dichloride/methylaluminoxane as a catalyst. *Macromol. Rapid. Commun.* **1999**, *20*, 419-422; (s) Byun, D.-J.; Kim, S. Y. Selective Chain Transfer Reactions in Metallocene Catalyzed Copolymerization of Ethylene with Allylbenzene. *Macromolecules* **2000**, *33*, 1921-1923; (t) Barsties, E.; Schaible, S.; Prosenc, M.-H.; Rief, U.; Röll, W.; Weynand, O.; Dorer, B.; Brintzinger, H.-H. ansa-Metallocene derivatives XXXIII. 2-Dimethylamino-substituted bis-indenyl zirconium dichloride complexes with and without a dimethylsilyl bridge: syntheses, crystal structures and properties in propene polymerization catalysis. *J. Organomet. Chem.* **1996**, *520*, 63-68; (u) Przybyla, C.; Fink, G. Two different, on the same silica supported metallocene catalysts, activated by various trialkylaluminums - a kinetic and morphological study as well as an experimental investigation for building stereoblock polymers. *Acta Polymerica* **1999**, *50*, 77-83.

3. (a) Kulangara, S. V.; Jabri, A.; Yang, Y.; Korobkov, I.; Gambarotta, S.; Duchateau, R. Synthesis, X-ray Structural Analysis, and Ethylene Polymerization Studies of Group IV Metal Heterobimetallic Aluminum-Pyrrolyl Complexes. *Organometallics* **2012**, *31*, 6085-6094; (b) Dias, A. R.; Ferreira, A. P.; Veiros, L. F. Bonding Geometry of Pyrrolyl in Zirconium Complexes: Fluxionality between σ and π Coordination. *Organometallics* **2003**, *22*, 5114-5125; (c) Dias, A. R.; Veiros, L. F. Are cyclopentadienyl complexes more stable than their pyrrolyl analogues? *J. Organomet. Chem.* **2005**, *690*, 1840-1844; (d) Heys, P. N.; Odedra, R.; Kingsley, A.; Davies, H. O. Hafnium and zirconium pyrrolyl-based organometallic precursors and their use for preparing dielectric thin films. WO2009155520A1, 2009; (e) Hsu, J.-W.; Lin, Y.-C.; Hsiao, C.-S.; Datta, A.; Lin, C.-H.; Huang, J.-H.; Tsai, J.-C.; Hsu, W.-C. Zirconium complexes incorporated with asymmetrical tridentate pincer type mono- and di-anionic pyrrolyl ligands: mechanism and reactivity as catalytic precursors. *Dalton Trans.* **2012**, *41*, 7700-7707; (f) Huang, J.-H.; Kuo, P.-C.; Lee, G.-H.; Peng, S.-M. Synthesis and structure characterization of 2-(dimethylaminomethyl)pyrrolate and 2,5-bis(dimethylaminomethyl)pyrrolate zirconium complexes. *J. Chin. Chem. Soc.* **2000**, *47*, 1191-1195; (g) Kaushik, N. K.; Bhushan, B.; Sodhi, G. S. Dithiocarbazate complexes of titanium(IV), zirconium(IV) and oxomolybdenum(VI) derivatives. *Indian J. Chem., Sect. A* **1981**, *20A*, 625-626; (h) Sodhi, G. S.; Kaushik, N. K. Oxinate chelates of cyclopentadienyl- or indenylzirconium(IV) and their halide salts. *Bull. Soc. Chim. Fr.* **1982**, 45-48; (i) Sodhi, G. S.; Kumar, S.; Kaushik, N. K. Dithiocarbamate anions as salts of oxinate chelates of zirconium(IV). *Acta Chim. Hung.* **1983**, *114*, 329-335; (j) Sharma, A. K.; Kaushik, N. K. Syntheses of (π-fluorenyl) and (π-pyrrolyl)thallium(I) and their group transfer reactions with trichloro(π-cyclopentadienyl)titanium(IV)/trichloro(π-cyclopentadienyl)zirconium(IV). *Acta Chim. Hung.* **1984**, *116*, 361-365; (k) Zhao, W.; Xu, X.; Yi, J.; Jing, X.; Chen, W. Olefin polymerization catalysts of Group IV metal complexes with pyrrole ring-containing ligands. CN1317500A, 2001.

4. Busico, V.; Cipullo, R.; Cutillo, F.; Friederichs, N.; Ronca, S.; Wang, B. Improving the performance of methylalumoxane: a facile and efficient method to trap "free" trimethylaluminum. *J. Am. Chem. Soc.* **2003**, *125*, 12402-12403.

5. APEX2, Version 2 User Manual, M86-E01078, Bruker Analytical X-ray Systems, Madison, WI, June 2006.

6. Sheldrick, G.M. "SADABS (version 2008/l): Program for Absorption Correction for Data from Area Detector Frames", University of Gottingen, 2008.

7. Dolomanov, O. V.; Bourhis, L. J.; Gildea, R. J.; Howard, J. A. K.; Puschmann, H. OLEX2: a complete structure solution, refinement and analysis program. *J. Appl. Crystallogr.* **2009**, *42*, 339-341.

8. Sheldrick, G. M. A short history of *SHELX*. *Acta Cryst.* **2008**, *A64*, 112-122.

9. Brandenburg, K. (1999), DIAMOND. Crystal Impact GdR, Bonn, Germany.

10. Spek, A. L. Structure validation in chemical crystallography. *Acta Cryst.* **2009**, *D65*, 156-168.